The Pennsylvania State University

The Graduate School

Engineering Design, Technology, and Professional Programs

IMPROVING QUALITY OF MULTI-FUNCTIONAL STRUCTURES CREATED VIA MATERIAL EXTRUSION ADDITIVE MANUFACTURING

A Thesis in

Engineering Design

by

Swapnil Sinha

Submitted in Partial Fulfillment
of the Requirements
for the Degree of

Master of Science

May 2017

The thesis of Swapnil Sinha was reviewed and approved* by the following:

Nicholas A. Meisel
Assistant Professor, Engineering Design and Mechanical Engineering
Thesis Advisor

Timothy W. Simpson
Paul Morrow Professor of Engineering Design and Manufacturing
Faculty Reader

Sven G. Bilén
Professor of Engineering Design, Electrical Engineering, and Aerospace Engineering
Head, School of Engineering Design, Technology, and Professional Programs

*Signatures are on file in the Graduate School

ABSTRACT

This work is motivated by Additive Manufacturing's (AM) ability to create multi-functional components via in-situ embedding. The layer-by-layer material addition approach gives designers access to the entire volume of a part, enabling embedding of foreign, multi-functional components within printed parts. The typical embedding process for AM involves i) designing the cavity for the embedded component, ii) interrupting the build process when the top layer of the cavity is reached, iii) manually inserting the foreign component, and iv) resuming the build process. While build process interruption during printing is a requirement for embedding, interruptions can also be caused by power outages, system errors, or material shortages. However, the influence of this interruption on AM manufactured parts is not well understood. This thesis discusses the effects of the embedding process on the material properties of material extrusion parts by addressing two different factors: i) the time duration of process interruption in a print and ii) the material transition between the embedded component and the build material when resuming the print after embedding. The information on how these two factors influence material properties can provide crucial information for designers to make design and process decisions for embedding in AM. For this purpose, the tensile strength of 3D-printed specimens with embedded elements was tested in this study, subjected to different pause time intervals, and with or without shape converters. Shape converters are the parts designed to fill the gap in the cavity after inserting the embeds, to create a flush surface before resuming the print. In order to counteract any weakness due to pausing, specimens in additional testing were reheated at the paused layer immediately prior to resuming, and

tensile strengths were analyzed to observe any differences. The findings from these investigations are used as design guidelines for redesign and manufacturing of a multifunctional cross brace structure of a three unit CubeSat.

TABLE OF CONTENTS

LIST OF FIGURES

LIST OF TABLES

ACKNOWLEDGMENTS

I would like to thank everyone who has guided and motivated me to achieve this degree. I give special mention to:

Dr. Nicholas Meisel, for accepting me into your lab, and for giving me the opportunity to learn and explore the new field of additive manufacturing. I am thankful for your unending support and guidance throughout the length of this research.

Dr. Sven Bilén, for your insightful inputs to my research and for letting me use the facilities of the Engineering Design Program.

Dr. Timothy Simpson, for providing me with your expertise in this field of study.

All members of the MADE BY DESIGN Lab, past and present, for being there and letting me borrow your expertise in solving problems.

My friends at Penn State for making this easy through your friendship and moral support.

Mumma, Papa, and Swastik for everything and for being there unconditionally.

Chapter 1

INTRODUCTION AND MOTIVATION

1.1 Motivation for Design for Additive Manufacturing (DfAM)

A product's design and innovativeness are directly related to its marketability, i.e., appeal to customers, and to its ability to generate profit [1]. Therefore, design tools and frameworks that allow designers to be more efficient, effective, and creative during the design process are of significant interest [2]. In order to generate profit, it also is essential to design these products such that they can meet manufacturing constraints, which helps to minimize production time and overall cost. Traditional manufacturing processes like injection molding, machining, forming, and joining may impose limitations on manufacturability, which limits designer ideation during the design process. For example, complicated parts may require special setups and incur high initial cost, or process types may introduce design constraints that force a product to be manufactured in different pieces and then be assembled. Parts that make up the product have to be designed for manufacturability, assembly, and possibly disassembly to effectively reduce part count, process time, and total cost incurred [3]–[5].

For over a century, Design for Manufacturing techniques have been implemented for traditional manufacturing methods in manufacturing industries [6]. For past few decades, Design, Theory and Methodology (developed by Reigeluth) has guided designers to achieve feasibility and efficiency in manufacturing [7]. However, recent advances in additive manufacturing (AM, also known as 3D printing) have introduced a completely new challenge to these methodologies because of its unique set of manufacturing opportunities [8]. AM's ability to control the properties of any point in a part's

geometry gives it the ability to create virtually any geometry imaginable, which allows designers to realize the creative ideas that were not previously feasible or prohibitively costly or complex.

AM technology has recently increased in popularity due to its simplicity, accessibility, and applicability, and it is also driving evolution in the traditional design process. This has created a demand for design guidelines specifically to support AM. This field of study, denoted Design for Additive Manufacturing (DfAM), develops guidelines to assist in tailoring designs for manufacturing using AM technology. DfAM aims to help explore the vast design space offered by AM [5] and helps to create an understanding of the relationship between the manufacturing process, designed structure, and material behaviors. The understanding of these influences is necessary to appropriately leverage the opportunities offered by AM. DfAM also addresses the restrictive side of AM: limitations in AM related to available materials, their performance, and their properties [8]. Restrictions can also include manufacturability-related limitations, such as the need for support structures, the use of post-processing, and the presence of layer stepping. The exact form of each of these restrictions is unique for each AM process type [8]. This thesis aims to address one particular restriction of DfAM: the influence of the in-situ embedding process on material properties.

1.2 Embedding Process with Material Extrusion (AM)

As an inexpensive and relatively easy-to-use process, material extrusion, also known by the trademarked term Fused Deposition Modeling (FDM), is one of the most common and widely used types of AM [9–12]. In material extrusion, a heated nozzle melts, extrudes, and deposits a fed thermoplastic filament on a build tray in a prescribed geometry. Solid layers are generated by side-by-side deposition and solidification of molten roads of thermoplastic. The build tray is lowered or the nozzle raised once a layer is completed. The next layer bonds with the previous layer as it cools

down. The control of the thermal environment is important for the successful bonding of roads; hence, the system is often enclosed to maintain appropriate temperature below the melting point of the material being extruded (see Figure 1-1) [13].

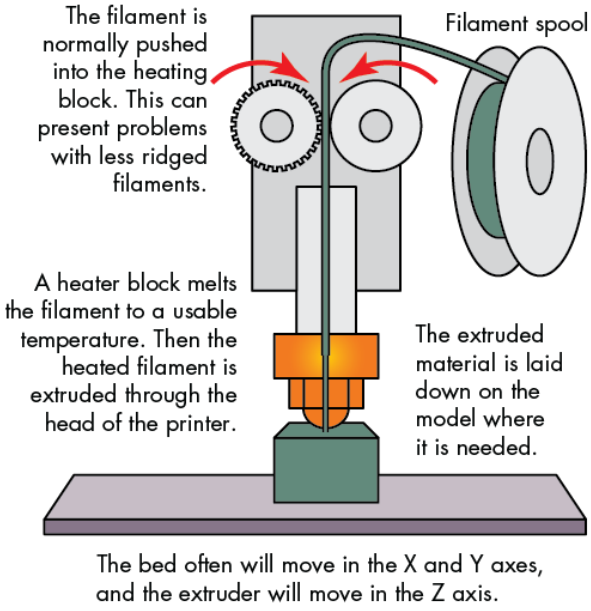

Figure 1-1. Material extrusion process, in which a heated nozzle liquefies plastic filament and extrudes it on a build tray [14].

Contrary to traditional subtractive manufacturing methods, the layer-by-layer nature of AM allows for access to the entire volume of the work piece throughout the build process. The layer-by-layer nature also provides an opportunity to embed sensors, actuators, circuits, and other functional components within a part during the manufacturing process [15, 16]. This embedding capability recently has been recognized for its application to the design and production of optimized parts and sophisticated “smart” objects [17–19]. However, AM is a relatively nascent method of manufacturing that cannot use the established standard design guidelines created for centuries-old traditional manufacturing processes. To realize the opportunities that AM promises in design and

manufacturing of multi-functional components, this work seeks to address this particular gap of information in DfAM - embedding.

1.3 Research Goals

Typically, the embedding process in AM involves 1) designing the cavity for the embedded component, 2) pausing the print when the top layer of the cavity is reached, 3) inserting the component, and 4) resuming the printing process [16]. While in-situ embedding is a powerful tool for AM, there are two factors that may greatly affect the strength of these embedded parts: (i) build process interruption and (ii) the material transition between the embedded component and the resumed layer. Since thermal environment control is crucial for bonding [13], an interruption in the process causes the top layer to cool down and may affect the layer bonding when resumed. The material transition occurs when the printing is resumed after embedding of a foreign component. The cavity is filled with the component, and the resumed layer is deposited on top of it. While qualitative observation notes that the layer adhesion may be impacted by both of these factors, their effects on the overall strength of the part are unknown. In this research, these effects on the strength of material extruded parts were studied experimentally by performing tensile testing on prepared material extrusion specimens of different treatment types. This information plays a crucial role for designers and researchers alike, for a careful and informed design of multifunctional components with AM.

1.4 Thesis Overview

To achieve the aforementioned research goals, this thesis presents a background on relevant research work and applications in Chapter 2, which lead to the motivation for the particular

approach employed in this research. Specifically, it looks into applications of multi-functionality, as well as AM processes that were used for achieving them. It also summarizes previous literature on design for embedding considerations. Chapter 3 elaborates the design of the experimental approach to answer the research questions. It provides a detailed reasoning for every step of the experiment. Chapter 4 presents the statistical analysis and summarizes the findings to answer the research questions. It also discusses the implications of the findings on design guidelines for AM. Chapter 5 presents a case study, which uses the suggestions for design guidelines in Chapter 4, to demonstrate its applicability in design and manufacturing of a multi-functional component. Chapter 6 summarizes the findings and concludes the thesis.

Chapter 2

LITERATURE REVIEW

2.1 Introduction

Previous research related to embedding with AM is presented in this chapter in three parts. Section 2.2 explores the diverse applications of the embedding process. Section 2.3 summarizes prior efforts in embedding materials using different AM process types. Section 2.4 outlines the existing research on design for embedding considerations, as well as mechanical properties of embedded parts.

2.2 Multifunctional Parts via AM, Applications of Embedding Process

The recent explosive growth of the Internet of Things [20] has spurred AM research on the validation of form with functionality, which primarily involves embedding functional components in parts [22–25]. Technologies such as near-field communication, real-time localization, and feedback from embedded sensors have enabled the transformation of everyday objects into "smart" objects. These objects are aware of their surroundings and can communicate or react accordingly [26, 27]. Isanaka and co-authors [27] summarized the use of embedding via AM technologies to help establish a Cyber-Enabled Manufacturing (CEM) environment. The CEM environment is a smart manufacturing environment that consists of a network of embedded sensors coupled with control systems to effectively gather information and offer immediate response in manufacturing facilities. AM makes embedding these sensors feasible and cost-effective. Integrating current technologies with AM allows for the design and production of sophisticated products in a CEM-like automated manner and, therefore, with a reduced product development cycle time [21], [28].

One of the major applications of multi-functionality is structural health monitoring (SHM), which is an emerging method for non-destructive product evaluation. It requires sensors to be embedded into a structure to capture, log, and analyze real-time data about the health of the structure. The benefits of this application are realized in structures like bridges, buildings, aircraft, and mega machines in which catastrophic failures must be avoided [29]. Strantza and co-authors [30] evaluated the performance of SHM systems embedded via AM for their suitability in the non-destructive testing of structures. The system was found to be reliable and is expected to be used to obtain a novel approach to structural design that relies on lightweight structures. These potential application areas for in-situ embedding via AM often require high safety and performance standards, as well as require careful process and quality control. Suitable standards for testing will ensure the acceptance of this emerging technology [31].

2.3 Embedding in Different AM Process Types

Layer-by-layer material addition allows for in-situ embedding applications to be realized in a wide variety of AM process types. A significant amount of the research on embedding via AM has been done with the Stereolithography (SLA) process, a vat photopolymerization AM technology [23]. Kataria and Rosen [32] demonstrated methods for fabricating embedded complex devices via SLA. Macdonald and co-authors [21] developed an SLA process to 3D print electronics, leading to reduced product development time. SLA has also been used to fabricate a new generation of sensors that use multiple surface interconnections to connect embedded electronics [33]. The process allows designers to use the product's volume in a more efficient manner, which helps reduce the overall size and weight of these circuits. This application has motivated researchers to investigate the high value manufacturing of satellites with both a mechanical structure and integrated electronics [34]. 3D-printed sensors and electronics have been considered for a space vehicle

project dubbed the ‘CubeSat Trailblazer’ [35] which has been commissioned by NASA and was launched in November 2013 [36]. However, a lack of durability was noted [19] due to the poor material properties of the photopolymer resin, which is the material used for fabrication in the SLA process [28].

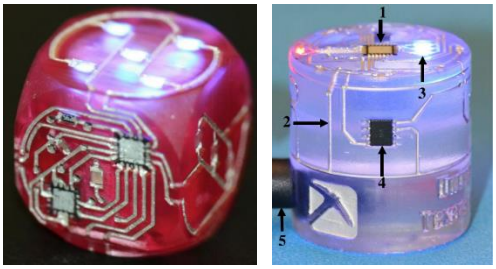

Figure 2-1. Examples of SLA fabricated embedded multifunctional components. (a) A 3D printed gaming die, with embedded electronics to sense motion, developed by Macdonald et al. [21]. (b) A novel magnetometer designed for SLA process for applications in small sized satellites [33].

When considering embedding within metal structures, traditional powder metallurgy processes involve isostatic pressing and diffusion bonding and can reach temperatures up to 565 °C. These high temperatures can prove damaging for sensitive embedded components, which has limited its usefulness in embedding applications [38]. In the area of metal powder-bed fusion AM, Rodriguez and coauthors [39] measured the printing surface temperature of the electron beam melting process by embedding a thermocouple in the build plate. The electron beam can cause the temperature of the metal surface to reach 2269 °C [40], making it impossible to insert temperature sensitive components. The sheet lamination process, ultrasonic additive manufacturing (UAM), is a solid-state joining process in which thin metallic tapes are ultrasonically welded on top of one another and periodically machined to create a final part [41]. Hahnlel and co-authors [38] demonstrated a successful electrical insulation of embedded material through UAM process on aluminum matrix composites. The parts fabricated through this process experience temperatures that stay below 25

°C and, therefore, the process is safe for embedded components like smart materials or sensors. However, UAM has had limited success bonding dissimilar materials, limiting its application in the aerospace, automotive, electrical, and power generation industries, where multi-material bonding is a requirement [42].

The material jetting process is an AM technique that utilizes drop-on-demand inkjet printing to selectively deposit droplets of photopolymer directly onto a build platform. Because of the low working temperatures and direct material addition layer after layer, this process is well-suited for component embedding. The material jetting process is capable of multiple material deposition, which allows for printed structures that exhibit variable properties like flexibility and rigidity. Meisel et al. [16] demonstrated procedures for creating actuated joints by embedding shape memory alloys, which involved exploring design for embedding considerations with the material jetting process. However, the print head assembly block passes over the printed part at a clearance of only 100 microns; any protrusions from the embedded component can cause damage to the nozzle. Also, there is a limited number of photopolymeric materials available for material jetting. As with SLA, this type of material results in fragile parts.

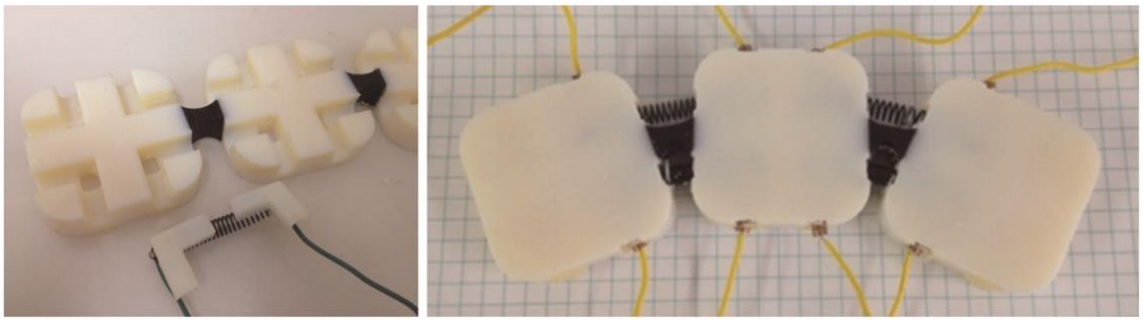

(a) (b)

Figure 2-2. Manufacturing of actuated joints by embedding shape memory alloys [16]: (a) shows the print immediately before embedding, with a shape converter for creating flush surface before resuming the print; (b) shows the final part with embedded functional components including a spring and shape memory alloy.

Polymer material extrusion is the one of the least explored, but also potentially the most useful and versatile, AM process types for in-situ embedding. With proper clearance design, components can be embedded without subjecting them to damaging temperatures and pressures. While inherent limitations of material extrusion make it difficult to produce geometries with tight tolerances or products with a fine surface finish, this limitation can be circumvented by its ability to embed highly finished parts. For example, standard components like bearings and shafts can be embedded in the material extrusion part, eliminating the concern of tolerances for fit or assembly [43]. Sbriglia and co-authors [44] embedded sensors in a material extrusion part to analyze the effects of operational process parameters on the quality and repeatability of parts being built. The study concurred with the findings of Stark and co-authors [45] about embedding sensors in FDM parts as a useful method for state-of-health monitoring in deployed systems. Aguilera and co-authors [22] demonstrated an integrated process for embedding high performance conductors directly into the thermoplastic material extrusion substrate to show the possibility of printing a complete electromechanical system in one build (see Figure 1-4). The wide variety of hybrid processes and thermoplastics available for material extrusion help to enable its wide application in various industries and make it a suitable candidate for in-situ embedding research.

The Mark One 3D printer by MarkForged is a 3D printer capable of creating carbon fiber-reinforced thermoplastic parts via dual extrusion of a Nylon base material with inclusion of continuous carbon fibers [46]. This combination of polymer printing with continuous carbon fibers enables users to create physical objects with high strength-to-weight ratios; the prints are claimed to be twenty times stiffer and five times stronger than standard ABS plastic [47], making it practical to produce high strength polymer parts with AM. With the printer, users can also preselect a layer and insert a pause while preparing the 3D model for printing. The print bed reregisters with 10-micron accuracy, allowing users to pause a print, remove the bed, add components, reinsert the bed,

and then continue the print with a high degree of precision. This focus on in-situ embedding in AM gives the Mark One an advantage over similar desktop material extrusion systems and makes it a well-poised candidate for a study of the impacts of in-situ embedding within AM.

2.4 Design for Embedding Considerations and their Impact on Material Properties

For producing a successful print with embedded components, certain design considerations are required before starting the manufacturing process. These design-for-embedding considerations were first demonstrated by Kataria and Rosen [32] for the SLA process. As shown in Figure 2-3, the SLA poses some limitations to embedding.

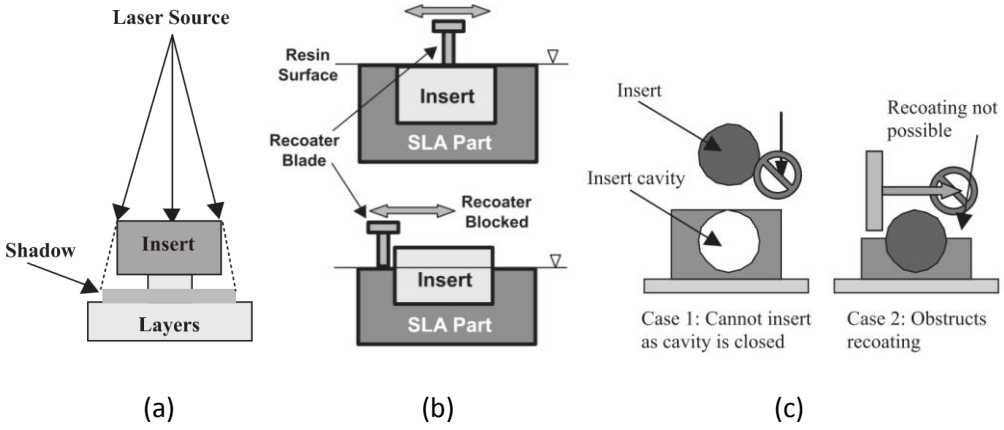

Figure 2-3. Demonstration by Kataria and Rosen [32] justifying design for embedding considerations for SLA; (a) shows how laser can be blocked by a foreign embed or insert, (b) shows how the protruded insert can obstruct the recoater, and (c) shows how round surface or similarly shaped inserts cannot be inserted or embedded by directly designing a negative cavity

Kataria and co-authors also suggested several design guidelines for embedding. Figure 2-4 shows one such suggestion in which the concept of shape converters was introduced for embedding an irregular geometry. Shape converters are parts that are designed to be embedded with components with irregular surfaces. This helps to create a flush surface at the paused layer. Shape

converters make sure that the resumed manufacturing process is not affected by the presence of the embedded component and vice versa.

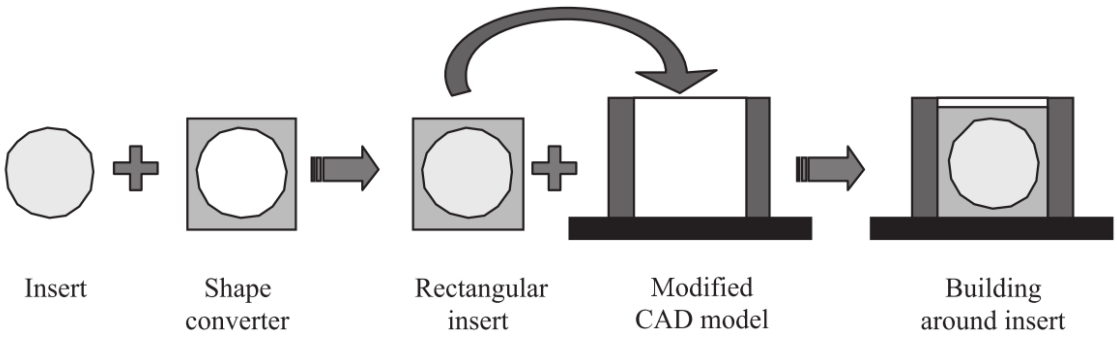

Figure 2-4. Step by step process for design for embedding which addresses the problem demonstrated in Figure 2-3 (c), in embedding a round geometry [32].

Similarly, Meisel et al. [16] addressed design for embedding considerations when embedding a long fiber in nonlinear channels with the material jetting process. During embedding, the fibers have the tendency to "pop out" of the embedding plane in such channels, which results in long embedding times and poses problems like obstructing the print head. The channels were redesigned to incorporate an overhang right above the cavity to hold the fiber in place (the original and redesign of the channel are shown in Figure 2-5 (a) and (b). Meisel et al. also demonstrated the design of a vertical post in the part in order to secure the fiber with a crimp at its ends. This shows that for ease of manufacturing, the components to be embedded can also be considered for redesign, along with the redesign of structures into which they are being embedded.

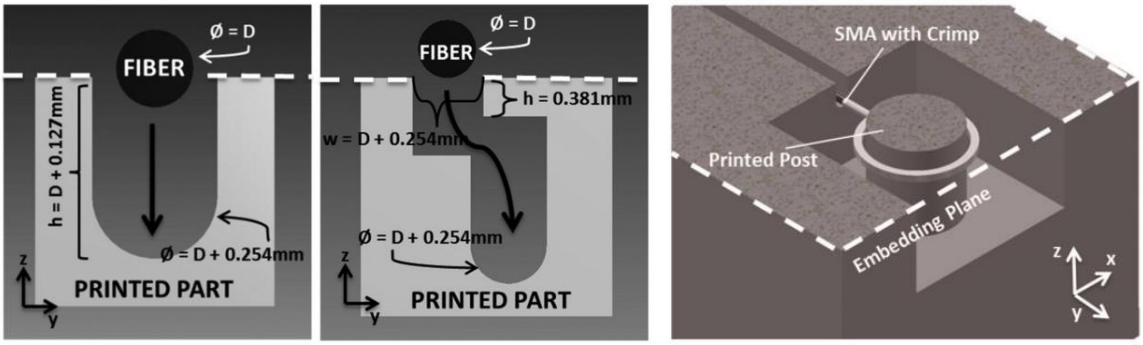

(a) (b) (c)

Figure 2-5. Shows the (a) the original channel design, (b) redesign of the channels to keep fiber inside the plane, and (c) a post, designed in the part to keep the fiber intact [16].

For the material extrusion process, Aguilera et al. [22] explored a design process for 3D printing an electric motor with components in it. The overall design was found to be volume- and material-efficient. Since the material extrusion system used by the authors (uPrint Plus) did not allow them to control the removal or addition of support material, support material could only be avoided when the roof of the cavity was at a 45° angle from the plane of the bed. This design guideline was used to design the cavity for embedding the motor components (see Figure 2-6).

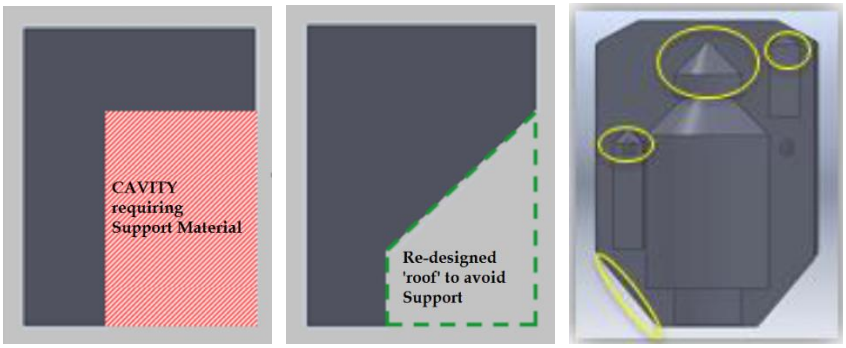

(a) (b) (c)

Figure 2-6. Panels (a) and (b) show the removal of support material from the cavity on redesign of the roof to 45° from the plane; (c) shows the application of the guidelines to redesign the cavity in the electric motor structure [22].

Aguilera et al. illustrated that once the digital design was complete, the manufacturing was done by pausing the print every time a cavity was finished, inserting respective components, and resuming the print. The stepwise process of embedding is demonstrated in the Figure 2-7, where each segment shows the image of inserted component.

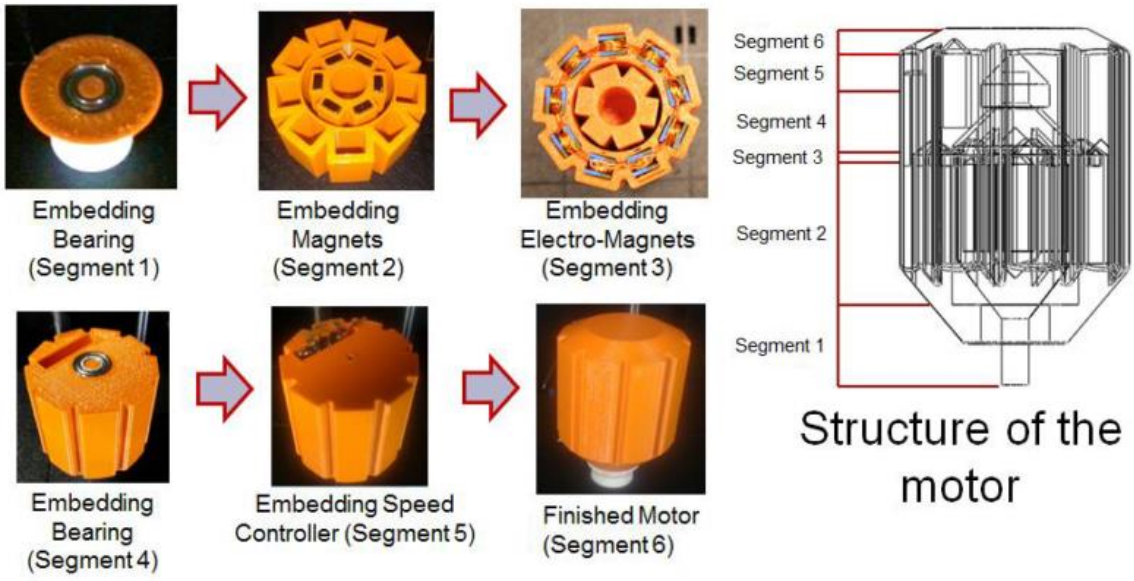

Figure 2-7. Manufacturing process of an electromechanical system (a motor) by in situ embedding with material extrusion process, each step of pause and embedding shown in segments [22].

Because inter-layer bond strength is a major factor when it comes to the mechanical properties of 3D printed parts [16], in-situ embedding has the potential to impact a structure's mechanical properties. However, a review of the available literature shows that published research in this area is still sparse. Klift et al. [48] performed tensile tests using the Mark One 3D printer to compare strength differences in two-layered (2CF) and six-layered (6CF) continuous carbon fiber embedded within a Nylon base. The tests revealed that discontinuities of the fibers led to premature failure in the areas where fibers were absen, and reduced the overall tensile strength of the composite

material. A further investigation of the 2CF and 6CF specimen cross-sections revealed that there was more void area in 6CF specimens. These voids had a negative impact on the elastic modulus of the composite, which calls for future work on the effects of different arrangements of carbon fiber layers on the mechanical properties of printed composites. Outside of AM, a study on the mechanical properties of cast epoxy resin with and without embedded silicon substrates verified that the ultimate tensile strength dramatically reduced when embedding was performed [49]. Also, the points of failure for each specimen were located at the embedded section. It was concluded that the strength of the part embedded with an insert will have to be investigated, if the insert possesses more rigid material properties [49].

As this review shows, the existing literature has demonstrated a consistent growth in acknowledgment of applications, process, and material property influences of embedding with AM. This has led to further investigations into processes that could assist in embedding. However, there is little to no research performed to understand the effects of process interruption or embedding on the mechanical properties of printed parts. To address this critical gap, this research investigates the effects of embedding on the material strength of the part. The research questions, hypotheses, and methodologies are discussed in Chapter 3.

Chapter 3

RESEARCH METHODOLOGY AND DESIGN OF EXPERIMENTS

3.1 Research Methodology

The objective in this research is to investigate the effects of the embedding process on the mechanical properties of material extrusion parts. To this end, tensile testing is used in order to determine i) how process interruption affects the strength of a printed part and ii) how the presence of an embedded artifact affects the strength of the printed part. When a print is interrupted, the exposed top layer loses heat to the atmosphere, causing the temperature of that layer to decrease. When the print is resumed, the first deposited layer bonds with the paused layer. This bonding may be affected by the reduction in temperature caused by the process interruption. Similarly, the bonding may be influenced by the material difference between the embedded component and the deposited material. After inserting the component, the exposed layer now has the embedded component's surface at the paused layer, which is then covered by the resumed material layer. To recreate the conditions of an uninterrupted print, the pauses layer is reheated to determine if that has any influence on part strength.

To scientifically investigate these hypothesized influences, experimentation was performed on specimens prepared accordingly. The process interruption specimens were prepared with different pause time intervals to test if there was any correlation between pause time interval and mechanical properties, while embedding specimens both with and without shape converters. Knowledge of the influence of these parameters can greatly benefit in making design decisions for manufacturing systems or for preparing safety critical parts.

Section 3.2 discusses the experimental setup and specimen design process. Section 3.3 discusses experimental setup and design of specimens with embedded components. Section 3.4

presents the process for determining clearances in specimen designs. Section 3.5 demonstrates the determination of clearances for embedded components and cavity designs. Section 3.6 shows the method for reheating the specimen in case of any weakness caused by the process interruption or embedding.

3.2 Process Interruption Experimental Setup and Specimen Design

As previously discussed, process interruption during 3D printing is a requirement while embedding, but these interruptions can also be caused by power outages, system errors, or material shortages. When dealing with such issues, the decision of whether to resume the print or to redo the print lies with the system user. While resuming the print saves time and material, it may affect the final part quality and properties. To make an informed decision, it is necessary to know the impact of this interruption on the strength of the printed part. To better understand these effects, a Mark One 3D printer is used to create specimens from nylon filament. The system can achieve a layer resolution of 100 microns, while Eiger (MarkForged's cloud-based, print preparation software [50]) gives a provision to insert a pause after any selected layer. This allows for a precise consistency in prepared specimens. All tested specimens were printed in a Z-orientation (See Figure 3-1) so as to study the magnified effects of process interruption on tensile properties of the parts.

(a) (b)

Figure 3-1. Build orientation of the specimen on Mark One and (b) Mark One while printing the specimen.

To perform tensile testing, first, a standard ASTM D638 specimen design was attempted for print [51]. However, the specimen dimensions were either too thin for a successful print or too tall to fit within the allotted build volume. The size of the cavity for the embedded component plays an important role in the success of the print; a constraint was introduced on the cavity's dimensions due to the printer's minimum feature size. An alternate tensile specimen design (see Figure 3-2 (b) and (c)) was selected based on the physical limits of the build platform, the potential for print success, and careful consideration of the parameters to be studied. The strength along the Z-axis is lower for material extrusion parts as compared to other build orientations. This material anisotropy is an inherent limitation of the material extrusion process, as material cools more thoroughly between layers than between roads, which affects fusion of the thermoplastic [52]. Therefore, all the specimens were printed in the Z-axis so as to study the magnified effects of process interruption on tensile properties of the parts.

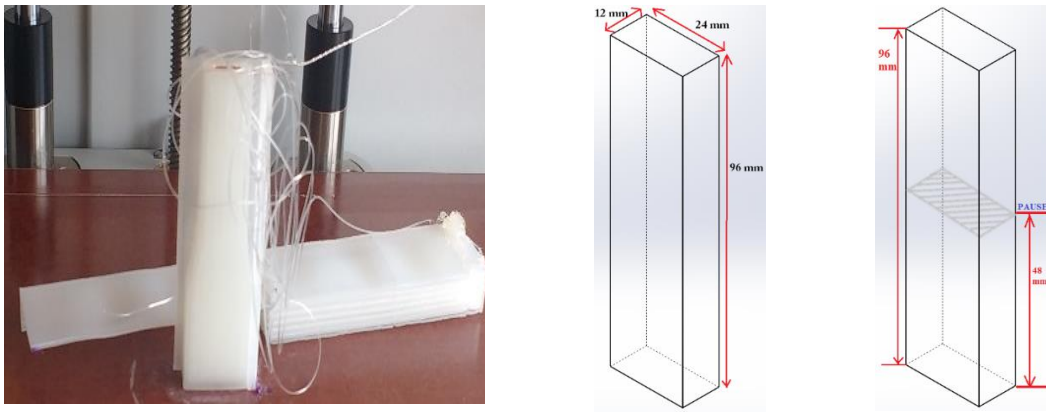

(a) (b) (c)

Figure 3-2. Shows (a) the failed print of a standard ASTM dog-bone sample design, (b) the final design of specimen for no pause, and (c) with pause of different time durations.

Process interruption for embedding purposes is required for the user to manually insert and secure the component. However, this process interruption cools down the paused layer with time. **It is hypothesized that the tensile strength of the specimen will be influenced by the time interval of pause due to the cooling of the paused layer**. For this purpose, specimens were prepared with different treatments of pause time intervals. Specimen design for no process interruption and process interruption is shown in Figure 3-2 (b) and 3-2 (c). The specimen with process interruption were paused at the middle layer for 5, 15, 30, and 60 minutes (see Table 3-1).

Table 3-1. Shows the specimens prepared with different treatment of time interval of pause, the tensile strength of these specimen was the metric used to compare these groups.

TREATMENT	No Process interruption	Process Interruption (Pause Time in minutes)			
3 Specimens each	0 mins	5 mins	15 mins	30 mins	60 mins

3.3 Embedded Specimen Experimental Setup and Specimen Design

The embedding process for a material extrusion part requires the user to manually insert the part to the designed cavity when the print pauses. Since the resumed layer is deposited on the paused layer, the paused layer must be flat in order to support the resumed layer and have a successful print. Therefore, when embedding a component with an irregular top surface geometry, a shape converter is used to cover the cavity at the paused layer and provide support to the resumed layer. While embedding components with flat surfaces may not require shape converters, the layer adhesion may be reduced due to the material transition between the top surface of the embedded object and the resumed layer of build material. **If a shape converter is used that is of the same material as the print material, it is hypothesized that it will improve layer adhesion between the paused and resumed layer, when compared to embedding a component without a shape converter**.

Specimens with different embedded components (copper tape and shape converter) were prepared to test the hypothesis and are shown in Figure 3.3. The two types of embedding specimens were designed with cavities of 5 mm × 11 mm cross-section and 0.5 mm depth for the copper tape specimen (see Figure 3-3 (a)), and 5 mm × 11 mm cross-section and 3 mm depth for the shape converter specimen (see Figure 3-3 (b)). The cross-section of the cavity was selected based on the success of the test prints as demonstrated in Section 3.2 (see Figure 3-2). The copper tape insert was selected because of its applications in direct writing of electronics with in-situ embedding and because of its smooth top surface. The shape-converter embedded specimen was designed with a 3 mm cavity depth in order to accommodate the added thickness of the shape converter, which is printed with the same system, parameters, and material as the specimen (see Figure 3-3 (c)). Three samples were printed for each of these treatment types.

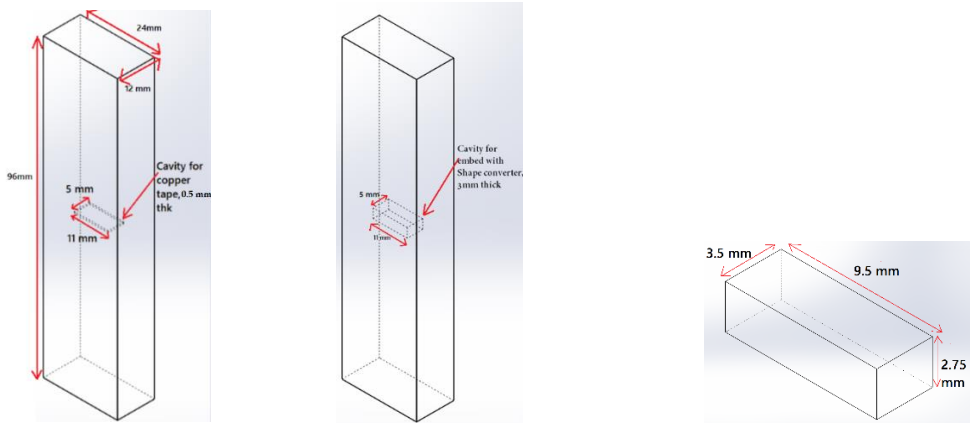

Figure 3-3. Specimen design for copper tape embed (a), and shape converter embed (b), with the dimensions of shape converter shown in (c).

Design dimensions and tolerances in AM are unique for each process type as well as each machine. Therefore, it is difficult to obtain standard designer's guidelines for any particular process or machine, especially given the relative youth of AM technology [53]. In order to properly dimension the shape converter, tolerances were obtained by experimentally determining appropriate clearances as elaborated on in Section 3.4.

3.4 Design Dimensions and Tolerances: Determining Clearance for Shape Converter

To determine the dimensions for the cross-section of the shape converter, a set of shape converters with digital design clearance values (the values in the SolidWorks™ V5 solid part file) varying from 0 mm to 2 mm in both the X and Y axes of the build were printed to find a perfect snug fit. An overly tight fit can cause residual stresses in the part and may influence the tensile properties of the overall part. A loose fit is to be avoided so that the embedded component does not move while the resumed layer is deposited. The shape converters of varying sizes were then inserted in the cavity of digitally designed 5 mm × 11 mm cross section, as shown in Figure 3-4. As shown

in Figure 3-4 (b), the shape converter with a design clearance of 1.5 mm in both X and Y axes was selected as having the most suitable tolerances for embedding. The selection was done on the basis of ease of fit and low clearance with the walls of the cavity.

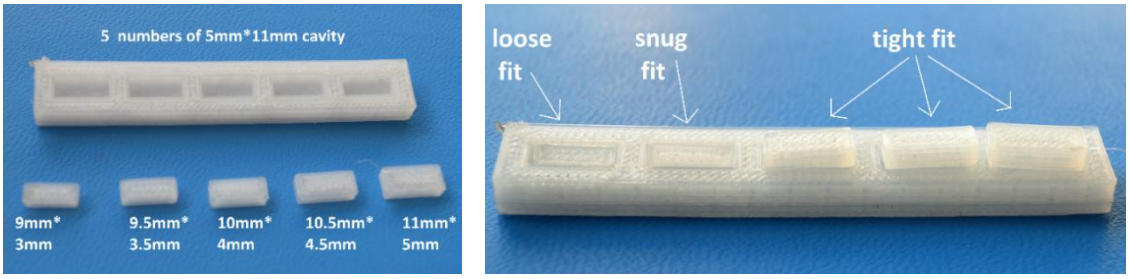

(a) (b)

Figure 3-4. (a) Initial shape converters with different clearance values varying from 0 mm to 2 mm in both X and Y axis and (b) demonstration that clearance of 1.5 mm in both X and Y axis was found to fit snuggly in the cavity.

To find the clearance for the shape converter in the Z-direction, another set of shape converters were prepared with the same cross-sections (chosen from the clearance test in X-Y plane, 9.5 mm × 3.5 mm) but with different thicknesses in the digital design (varying from 2 mm to 3 mm, as shown in Figure 3-5) to find its appropriate fit in a cavity designed with 3 mm depth. The alignment of the top layer of the shape converter was checked after inserting it into the cavity. This is important because the layer adhesion between the embedded component and the resumed layer would depend highly on the alignment of the shape converter with the paused layer; an indented shape converter will have low or no adhesion with the resumed layer, and a protruded shape converter can impact the nozzle and can damage the part or the printer. As shown in Figure 3-5 (b), the shape converter with a digitally designed Z-axis clearance of 0.25 mm was selected as having the most appropriate vertical clearance for the shape converter. As seen in the images, the cavity caused by the indented shape converters would not solve the purpose of inserting a shape converter

to improve strength and the protruded shape converter would be damaging for the print head if the print is resumed. The aligned specimen was chosen so as to find the effects (if any) of the inter-layer bond strength between the top layer of shape converter and the resumed layer. Therefore, the shape converter was designed with a final clearance of 1.5 mm on the X and Y axes each. The Z axis clearance was set at 0.25 mm so that the top plane of the shape converter coincides with the paused layer of the part, after being inserted in the cavity.

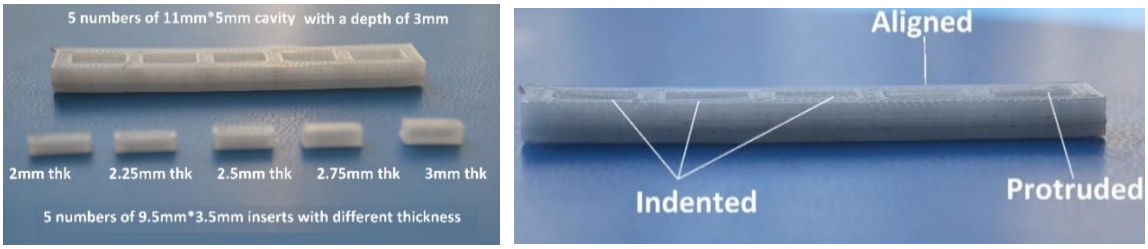

(a) (b)

Figure 3-5. (a) Initial shape converters of same cross sections but different thickness values, varying from 0 mm to 1 mm and (b) demonstration that the shape converter with a design clearance of 0.25 mm in Z axis was the most aligned with the top layer.

The shape converter of digitally designed dimensions **9.5 mm × 3.5 mm × 2.75 mm** was selected after checking for clearances.

3.5 Reheating the Partially Printed Specimen

As discussed in Section 3.1, one known event that occurs with process interruption is the cooling of the paused layer. Cooling of the extruded melt is necessary for the material extrusion process so that the next layer can be built on the solidified extrusion. However, this cooling between layers makes the part weaker along the Z direction, introducing material anisotropy in the part. Ravi et al. [54] attempted to create a material extrusion system with a near infrared (IR) based localized

heating method, to heat up the surface right before deposition. They were successful in increasing the inter-layer bond strength by 50%, which was caused by better diffusion of the heated layers.

In the case of embedding, the process of inserting a significant multifunctional component into a cavity typically takes at least 5 minutes of process interruption, which is enough time to lose most of the heat through convection and radiation to the atmosphere. In order to find the temperature of the immediately deposited layer, the temperature history (see Figure 3-6) of the print was measured via infrared (IR) imaging using an Optris Pi 400 IR camera and Optris Pi Connect process monitoring software (Optris Gmbh, Berlin, Germany). The temperature of the immediately deposited layer was calculated to be 96 °C (on average) (see Figure 3-7). **It is hypothesized that if the paused layer is reheated to the same temperature as that of an immediately deposited layer, then the conditions of an uninterrupted print can be recreated, thereby reducing the effects of the process interruption**.

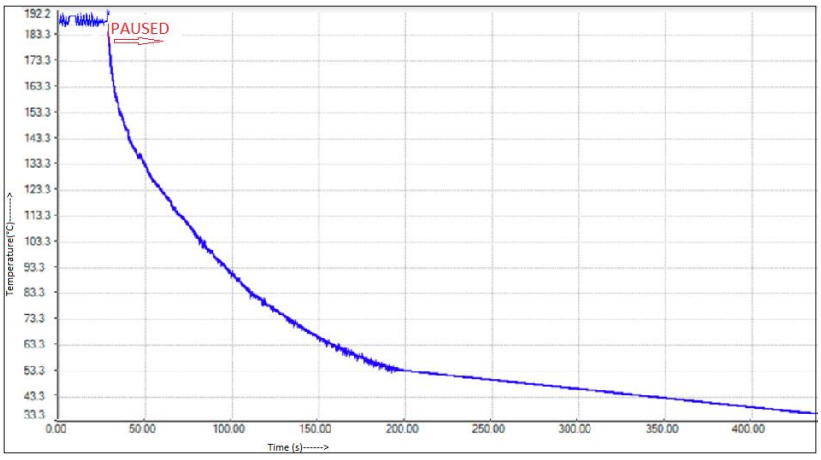

Figure 3-6. Temperature vs time diagram of the print before and after pausing, shows temperature loss for the surface layer with time, obtained with Optris Pi IR camera.

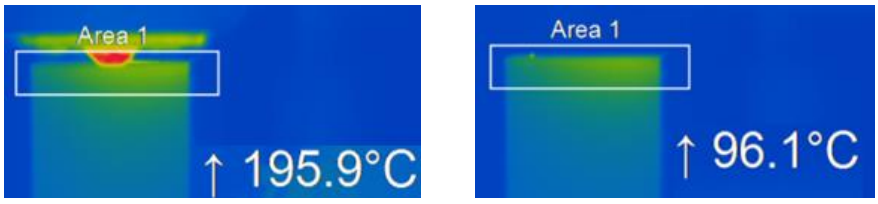

(a) (b)

Figure 3-7. A snapshot of specimen being printed with the temperature (a) of the printing nozzle & (c) of the most recent layer, through IR camera.

To test this hypothesis, the specimens were prepared in the same manner as the earlier process interruption and embedding treatment specimens. To make sure that the paused layer reaches room temperature, the pause time interval was kept at 15 minutes. The paused layer was then reheated to approximately 110 °C, and the print was resumed. By the time the actual deposition of the resumed layer started, the temperature of the paused layer was close to 96 °C. Specimens with i) 15 minute process interruption, ii) copper tape embedding, and iii) shape converter embedding were reproduced by reheating right before resuming the print. To reheat, a standard heatgun was set to 350 °C, and manually held approximately 10 cm above the paused layer, directed perpendicular to the paused layer. Three specimens for each treatment were prepared by reheating the paused layer, right before resuming the print, as seen in Table 3-2.

Table 3-2. Shows the specimens prepared with reheat treatment, at the paused layer.

REHETEAD Process Interruption (Pause time in minutes)	REHEATED Embedded	
15 mins	Copper tape	Shape converter

Chapter 4
TESTING, DATA ANALYSIS, AND DISCUSSIONS

4.1 Introduction

Chapter 3 elaborated the research methodology for this research work, where design for experimental approach was explained. This chapter elaborates the experimental details, data collection and analysis, and discusses the implications of the findings.

4.2 Testing Setup for All the Specimens

The build was prepared using MarkForged's Eiger software; key settings were 0.2 mm layer height, 100% fill density, and a rectangular fill pattern. Each specimen was printed individually and stored in a dark location at room temperature (24 °C) with 50% humidity. Desiccant packets were used in an attempt to control the impact of humidity. Tensile testing was performed after at least 48 hours of storage. Tensile testing was performed using an Instron 5866 Mechanical Testing Machine, using mechanical wedge action grips on a 5-kN load cell (see Figure 4-1).

Figure 4-1. Tensile testing on Instron 5866 Mechanical Testing Machine.

The pull rate was set at 5 mm/min. Serrated jaw faced grips of thickness range from 6.35 mm to 12.7 mm were used. Gauge length, width, and thickness of each sample was recorded in millimeters; every 0.1 second the extension (mm), tensile stress (MPa), load (N), and tensile strain (mm/mm) were recorded. The temperature during testing was recorded as 24 °C, and the humidity was recorded as 55%.

4.3 Effects of Process Interruption on Tensile Strengths of Parts

Gathered data were checked to ensure that they met the assumptions under which they were parametrically tested in order to validate the use of statistical analysis to identify significant differences. These assumptions are independence of cases, normality, and homogeneity of variances. All the assumptions were met except for normality. The Shapiro-Wilk test [55] confirmed that the data for maximum tensile stress is not normal ($p = 0.002, < 0.05$). Therefore, non-parametric tests were performed to analyze data for maximum tensile stress. The statistics of

the maximum tensile stress data obtained for each of the three specimens made for each treatment are reported in Table 4-1. Three specimens were tested for each treatment.

Table 4-1. Statistics of maximum tensile stress (MPa) values obtained for each treatment:

Treatment	*Mean*	*Median*	*Std. Deviation*	*Variance*	*Range*	*Minimum*	*Maximum*
0 minute pause	13.03	12.92	0.20	0.04	0.36	12.90	13.26
5 minute pause	7.43	7.90	1.42	2.01	2.72	5.84	8.56
15 minute pause	7.00	7.03	0.75	0.57	1.51	6.23	7.740
30 minute pause	6.27	6.13	0.69	0.48	1.36	5.66	7.02
60 minute pause	7.54	7.17	0.75	0.56	1.35	7.05	8.40

Since there are five groups (treatments) to be compared, a Kruskal-Wallis H test (also known as one-way ANOVA on ranks) [56] was performed to identify if there was any statistically significant difference in the data due to treatments. A Kruskal-Wallis *H* test is a rank-based nonparametric test used to determine if there are statistically significant differences between two or more groups of an independent variable on a continuous or ordinal scale. The test showed that there was a statistically significant difference in maximum tensile stress values between different treatments, $\chi^2(2) = 9.633$, $p = 0.047$, with a mean rank of 14.00 for no pause, 8.00 for 5-minute pause, 6.33 for 15-minute pause, 3.00 for 30-minute pause, and 8.67 for 60-minute pause. Effect size quantifies how well this difference works in a range of contexts [57]. This value can be calculated as:

$$\text{Effect size} = \chi^2/(N - 1) = 9.633/(15 - 1) = 0.688$$

where N is the total number of observations. The value 0.688 of effect size means that 68.8% of the variability in rank scores is accounted for by different treatments. The Kruskall-Wallis test only verifies that at least two groups were significantly different. To identify where these differences occurred, post-hoc analysis was performed by pairwise comparison of each combination of groups (based on treatment). To study the individual tensile property effects of process interruption while

embedding (pausing the print to insert) or due to system errors, the specimens prepared with pause were compared by grouping them on the basis of time interval of the pause. Specimens with no process interruption (0 minutes pause) were used as reference values for the analysis. The maximum tensile stress values are reported by the pause time intervals in Figure 4-2. Error bars indicate sample standard deviations of the data points for each treatment.

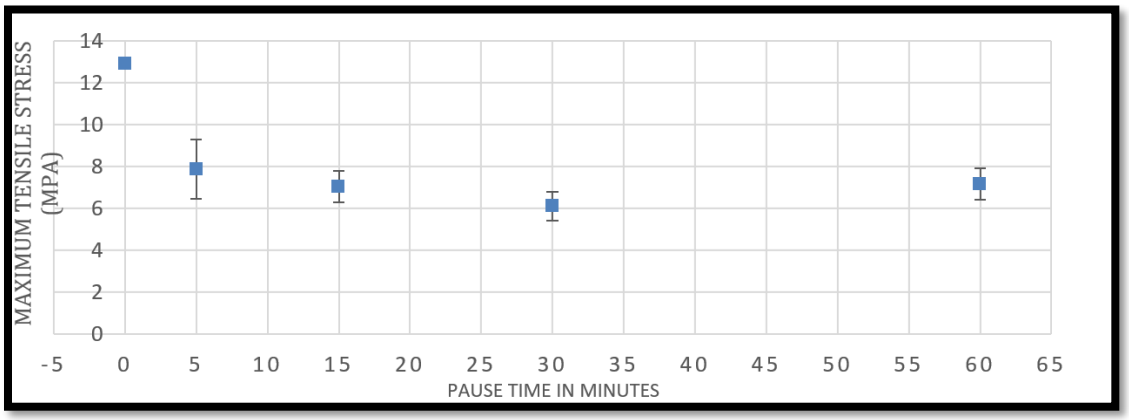

Figure 4-2. Median values of maximum tensile stresses of specimens with respect to their pause time

The graph shows a clear difference between maximum tensile stress values of specimens with process interruption (5, 15, 30, and 60 minutes of pause) and specimens without any process interruption (0 minutes of pause). However, there is no clear difference in maximum tensile stress values for specimens with different pause times (>0 minutes).

The post-hoc test performed on the data was the Mann-Whitney *U* test, which is a non-parametric test to compare two independent groups [56]. Pairwise *U* and *p* values for the Mann-Whitney *U* tests are shown in Table 4-2. Any *p* value of 0.05 or less has been highlighted to indicate statistical significance between the maximum tensile stress values. This test helps in identifying the specific differences that are significant, which could not be obtained using the earlier Kruskall-Wallis *H* test.

The Mann-Whitney *U* test indicated that the ultimate tensile strength was greater for specimens with no pause (Median = 12.917 MPa) than for specimens with a 5-minute pause (Median = 7.899 MPa), 15-minute pause (Median = 7.037 MPa), 30-minute pause (Median = 6.131 MPa), and 60-minute pause (Median =7.173 MPa). **This shows that process interruption does have a statistically significant effect on the tensile strength of the printed part.** Since there is no statistically significant difference between the maximum tensile stress when comparing all pause times greater than 0 minutes, experimentation suggests that the magnitude of pause time has no significant effect on the strength of the part. However, there is a statistically significant difference between maximum tensile stress values for 30-minute pause time versus the 60-minute pause time. This difference is inconsistent with results from the other pairs of pause time intervals; more data points are needed to confirm the exact reason for this difference.

Another interesting observation from tensile testing was related to the location of each specimen's failure (see Figure 4-3). Specifically, each interrupted specimen failed at the layer where it was paused (in this case, the center layer). Meanwhile, the layer of failure for specimens without any process interruption varied across the part. This confirms that process interruption introduces a notable weakness on the layer where interruption occurred. This information is important when designing functional AM components to be manufactured with in-situ embedding. The location of the embedding plane should be carefully determined considering the weakness introduced at it.

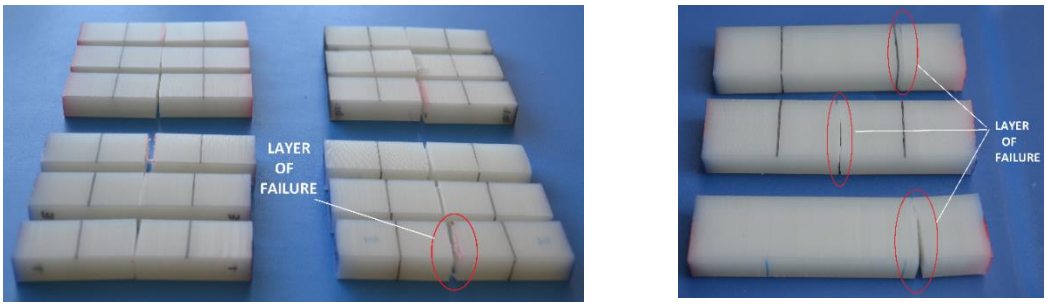

(a) (b)

Figure 4-3. Examples of specimen failure after testing with (a) process interruption specimens grouped based on time interval for pause, all failed at the layer which was paused, and (b) specimens with no process interruption, failed at varying layers.

4.4 Effects of Embedding, with and without Shape Converter

Since there was no influence on maximum tensile strength when the pause time was greater than 5 minutes, the three specimens with embedded components were prepared by pausing for 15 minutes immediately after the cavity was printed. Three embedded copper tape specimens were created by inserting a 5 mm × 11 mm piece of copper tape inside the designed cavity. The three embedded specimens with shape converters were prepared by inserting the designed shape converter (demonstrated in Section 3.4) into the printed cavity once its top layer was reached.

The tensile testing was performed with the same parameters as before. The statistics derived from the maximum tensile stress raw data for each treatment are reported in Table 4-2.

Table 4-2. Statistics of data obtained for maximum tensile stress values (MPa) for each treatment:

Treatment	Mean	Median	Std. Deviation	Variance	Range	Minimum	Maximum
No process interruption	13.03	12.92	0.20	0.04	0.36	12.90	13.26
Copper tape embed	5.28	5.12	0.96	0.92	1.90	4.41	6.31
Shape converter embed	5.11	4.97	0.68	0.46	1.34	4.50	5.84
With process interruption	7.54	7.17	0.75	0.56	1.35	7.05	8.40

As before, the data were checked to ensure they met the assumptions for parametric testing. A Shapiro-Wilk test (see Table 4-3) confirmed that the data for maximum tensile stress were not normal ($p = 0.014, < 0.05$). Therefore, non-parametric tests were performed to analyze the maximum tensile stress data.

The Kruskall-Wallis *H* test showed that there was a statistically significant difference in maximum tensile stress values between different treatments, $\chi^2(2) = 9.359$, $p = 0.025$, with a mean rank of 11.00 for no process interruption, 3.67 for the copper tape embed, 3.33 for the shape converter embed, and 8.00 for specimens with only process interruption. Effect size [57] was calculated as:

$$\text{Effect size} = \chi^2/(\text{N} - 1) = 9.359/(12 - 1) = 0.8508$$

The 0.8508 effect size value means that about 85% of the variability in rank scores is accounted for by different treatments. Pairwise statistical analysis (Mann Whitney *U* Test) was performed on the groups of treatments, to identify significant differences in maximum tensile stress. Pairwise *U* and *p* values for the test are shown in Table 4-3; any *p* value of 0.05 or less has been darkened to signify statistically significant differences between ultimate tensile stress values.

Table 4-3. Post hoc analysis results of pairwise comparison of groups with different embedding conditions, only process interruption, and no process interruption.

Condition	Process Interruption | Mdn = 7.044	Copper Tape embed | Mdn = 5.121	Shape converter embed | Mdn = 4.976
No interruption| Mdn = 12.917	0.05	0.05	0.05
Process interruption| Mdn = 7.044	-	0.05	0.05
Copper tape embed| Mdn = 5.121	0.05	-	0.827

The Mann Whitney *U* test indicated that the ultimate tensile strength for specimens with embedding (Copper tape embed Mdn =5.048 MPa, Shape Converter embed Mdn =4.976 MPa) is significantly less than specimens with only a pause (Mdn = 7.173 MPa), $U = 0$, $p = 0.05$. This can be explained by the presence of the cavity in the embedded specimens. Theoretically, the presence of a cavity in any material results in stress concentrations around the cavity, which makes that cross-section weaker. In addition, statistical analysis shows that the maximum tensile stress values of embedded specimens (Copper tape embed Mdn = 5.048 MPa and Shape converter embed Mdn = 4.976 MPa) are significantly lower than that of specimens with no process interruption (Mdn=12.917MPa), $U = 0$, $p = 0.05$. This difference is higher than the difference observed between process interruption and no process interruption in Section 4.2.

The Mann-Whitney *U* test also indicated that there is no statistically significant difference ($U = 4$, $p = 0.827$) between the ultimate tensile strength for specimens with only copper tape embedded (Mdn = 5.121 MPa) and for specimens with a shape converter embedded (Mdn = 4.976 MPa). While it is hypothesized that shape converters would provide increased adhesion between the last layer before embedding and the resumed layer, there was no practical improvement in the strength of the parts. This suggests that designers only need to use shape converters as the geometry of the embedded components requires them. Figure 4-4 below shows a plot of the median maximum tensile strength values obtained for each treatment.

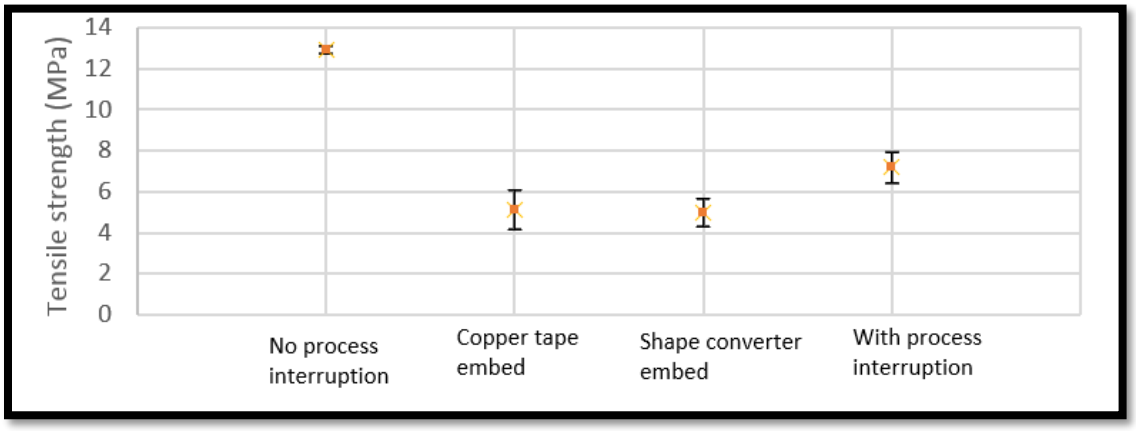

Figure 4-4. Median values of maximum tensile strength values for each treatment.

Overall, the presence of an embedded component causes a significant decrease in maximum tensile stress compared to that with only process interruption. A reduction of **70%** of the median stress value was observed. Additionally, the presence of a shape converter showed no significant effect on tensile properties as compared to an embedded component without a shape converter. The location of failure for the embedded specimen (see Figure 4-5) was same as that for the process interruption seen earlier. All of the specimens with any form of process interruption failed at the layer which was paused. Though the two types of embedded specimens had two different cavity depths (0.5 mm for copper tape embed and 3 mm for shape converter embed), the failure still occurred at the layer paused. This is important information for making design decisions; the location of the embedded component in a loaded part becomes crucial because of the weakness introduced by the paused layer as well as additional weakness caused by the presence of an embedding cavity in a material extrusion part.

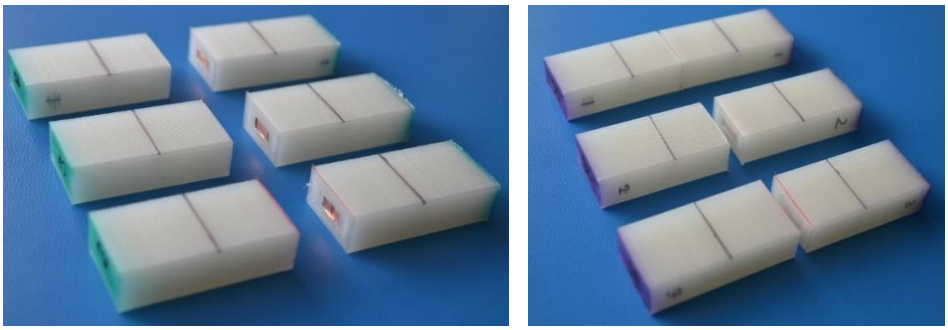

(a) (b)

Figure 4-5. After tensile testing, (a) copper tape and (b) shape converter embedding specimens with demonstrated failure at the pause layer

Experimentation and analysis suggest that the process of embedding significantly reduces the strength of the part because of two factors: (i) process interruption and (ii) presence of a cavity for embedding. Previous research on polymer diffusion has also suggested that the temperature change caused due to process interruption results in lower diffusion between polymer roads, which results in lower strength values [58]. Although one might assume that the use of a shape converter for embedding should assist in improving the adhesion between paused and resumed layers, experimentation demonstrated that this is not the case.

4.5 Addressing the Weaknesses: Reheat Treatment

During specimen preparation, it was observed that process interruption allows the top layer to cool down to room temperature within 5 minutes (see Figure 3-6). Results from Section 4.2 and 4.3 show that this greatly affects the strength of the parts. Therefore, to decrease this weakness introduced by process interruption, additional testing was performed in which specimens were reheated after process interruption according to the methods discussed in Section 3.5.

The reheated specimen tensile tests were performed with the same conditions as for specimens with process interruption and embedded components. The tensile strength values of these reheated

specimens were then compared with the values of their non-reheated counterparts (from Sections 4.2 and 4.3). As shown in Table 4-7, the Mann-Whitney *U* test indicated that the ultimate tensile strength was significantly higher ($p < 0.05$) for specimens reheated after a 15-minute pause (Median = 10.52 MPa) than for specimens with no reheating (Median = 7.037 MPa). The reheated copper tape (Median = 9.77) and reheated shape converter (Median = 9.31 MPa) embedded specimens also had significantly higher tensile strengths compared to their non-reheated counterparts ($p < 0.05$). This shows that reheating is able to significantly improve the strength of printed parts that have been subjected to some form of process interruption (with or without additional embedding). These findings were consistent with polymer diffusion findings by Bartolai et al.'s [58] weld theory of reduction in strength caused by reduction in diffusion due to temperature change.

Table 4-4. *p*-values for pairwise comparison of groups with different treatments. Grey background highlights the statistically significant differences. (Median value of strength in MPa reported as Mdn.)

Treatments	Process Interruption| Mdn=7.044	Copper Tape Embed| Mdn=5.121	Shape Converter Embed| Mdn=4.976	Reheated Process Interruption| Mdn=10.52	Reheated Copper Tape Embed| Mdn=9.77	Reheated Shape Converter Embed| Mdn=9.31
No Process Interruption| Mdn-12.92	0.05	0.05	0.05	0.05	0.05	0.05
Process Interruption| Mdn=7.044	-	0.05	0.05	0.05	0.05	0.05
Copper Tape Embed| Mdn=5.121	0.05	-	0.827	0.05	0.05	0.05
Shape Converter Embed| Mdn=4.976	0.05	0.827	-	0.05	0.05	0.05
Reheated Process Interruption| Mdn=10.52	0.05	0.05	0.05	-	0.827	0.513
Reheated Copper Tape Embed| Mdn=9.77	0.05	0.05	0.05	0.827	-	0.827

While improvement was seen when pieces were reheated, the specimens with no process interruption (Median = 12.917 MPa) were still significantly stronger than all other specimens. However, the reheat treatment did help improve the strength of the process interruption specimens by 47% and the embedded specimens by 90% (values as seen in Figure 4-6). The failure location for the reheated parts was still found to be the layer that was paused, just like the earlier specimens prepared without reheating. This indicates that reheating a paused specimen back to its initial

deposition temperature does improve the strength significantly, but it does not completely remove the weakness.

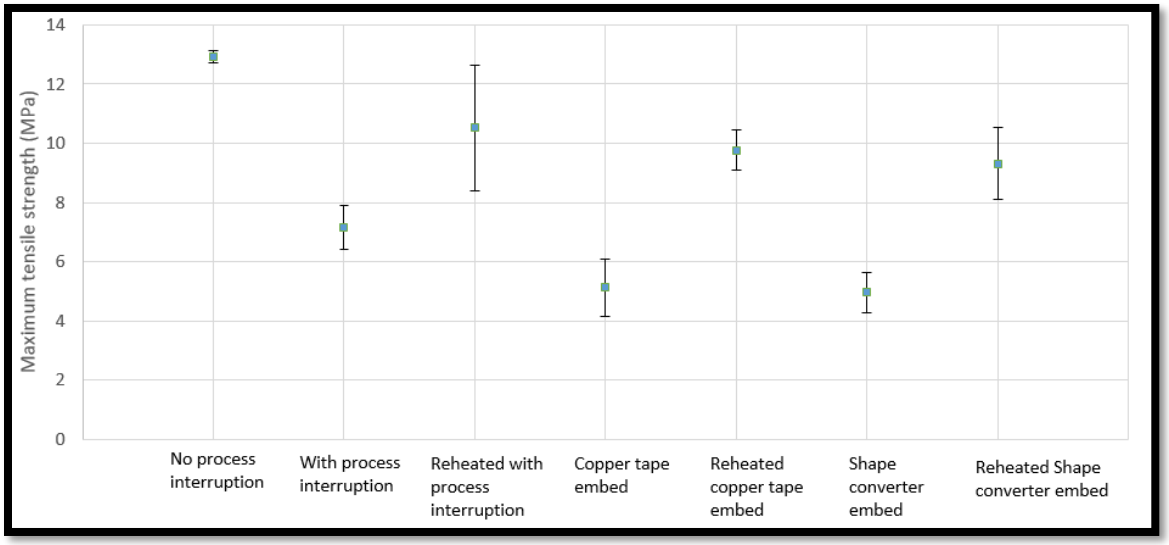

Figure 4-6. Median maximum tensile strength values for each treatment with error bars.

4.6 Suggestions for Design for Embedding Guidelines

The findings from Sections 4.2, 4.3, and 4.4, provide crucial information for designers to make decisions when creating multifunctional components by embedding with material extrusion AM. These findings are summarized as follows:

- In an event of unplanned process interruption, the designers should consider redoing the print for better part strength. The paused layer may be reheated before resuming in order to offset a portion the interruption effects, but this does not completely eliminate the weakness introduced.
- The cavity should be designed and placed in the part so that the layer paused for component insertion is not located at the load-critical points of the part. Reheating of the

paused layer should be considered for improving the strength of the part when embedding.

- The use of shape converters does not improve strength of the part; therefore, their use solely depends on the geometry of the foreign component being embedded.

In the next chapter, these suggestions were applied to a case study of creating a multi-functional part for a satellite.

Chapter 5

A CASE STUDY OF DESIGN FOR EMBEDDING WITH AM

5.1 Motivation for Application: Sun Sensor in CubeSat

The design guidelines suggested in Section 4.5 are based on the findings from experimentation summarized in Chapter 4. They apply only to the polymer material extrusion process because different AM processes pose different types of manufacturing restrictions on 3D printed parts. To demonstrate the applicability of these suggestions, the design and manufacturing of a multifunctional CubeSat satellite component was chosen as a case study.

Applications of AM multi-functionality are being realized in development of next-generation space exploration vehicles, in which versatile material options and manufacturability enable added volumetric efficiency [37, 57]. This is especially relevant when considering that the direct writing of conductive material has given designers flexibility to create circuits with efficient placement of components and higher manufacturing efficiency. Where traditional placement of electronics in a geometrically complex part is difficult, AM allows for fabrication of these electronics on conformal surfaces and in complex shapes. Therefore, the processes and materials for such applications are evolving at a rapid pace [29, 58].

CubeSat satellites are relatively inexpensive and small-dimensioned satellites that aim to increase university and researcher accessibility to space. A 1 unit, or 1U CubeSat has cubic dimensions of 10 cm × 10 cm × 10 cm, with mass less than 1.33 kg. The OSIRIS-3U (Orbital System for Investigating the Response of the Ionosphere to Stimulation and space weather) satellite is a 3U CubeSat that aims to study space weather [61]. A set of ***sun sensors*** integrated into the CubeSat can be used to identify the position of the Sun in order to obtain data to evaluate and manipulate satellite position or orientation [61].

Satellites in low Earth orbit can experience temperatures ranging from −40 °C to +80 °C. For this case study, a CubeSat sun sensor is used (Figure 5-1), which has an operating temperature range from −25 °C to +50 °C [62]. Therefore, a conduction-based heater is required to keep the sensor in the appropriate range operating temperature while in orbit. This heater can be designed and manufactured with the material extrusion process, due to the variety of conductive materials available for the process type. The next section explores the versatility of the conductive materials available for material extrusion, as well as experimental validation of one such material for 3D printing an embedded CubeSat heater.

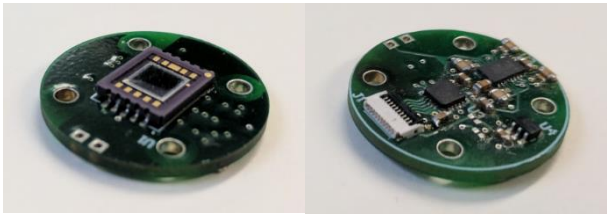

(a) (b)

Figure 5-1. The sun sensor (a) showing the receptor, and (b) showing the electronics on the other side of the circular circuit board, with the processing units.

5.2 Conductive Material for the Heater and Its Validation

As discussed previously, the material extrusion process has recently grown in popularity in multi-functional part creation because of its relative robustness and versatile materials [3, 61–63]. Most research until now has focused on improving material properties for creating mechanically sound structures [16, 49, 64–66]. However, the ease of producing polymers with infused metal or carbon fiber has developed a range of conductive thermoplastics [67–69]. Electrical characterization of these materials has shown the presence of anisotropy in heat and electrical conductance, which can be influenced and controlled by process parameters [67, 68].

Thermoplastic polymers like polylactic acid (PLA) and acrylonitrile butadiene styrene (ABS) are the most extensively used and commercially available material extrusion materials [71]. These polymers are often infused with additives or fillers to manipulate their material properties (e.g., thermal stability, conductance [70, 71], impact resistance [74], and elastic modulus [75]). To create conductive materials, additives like metal and carbon are added to a polymer base. Using these hybrid materials in material extrusion have shown losses in electrical conductivity due to orientation [68], layer thickness, raster width, and air gaps [69].

To design the printable CubeSat heater, commerciall-available conductive PLA material was first validated for the purposes of resistive heating. A sinusoid-like geometry was digitally designed and printed with a desktop-scale Lulzbot Taz 5 3D printer and conductive PLA material. The material (Composite PLA by Proto-pasta; electrically conductive graphite [76]) shows conductive behavior with a resistance of 2 kΩ in our printed geometry, which is an appropriate value for a resistive heating element. However, to properly design the heater, the material needs to be characterized based on process parameters, material properties, and part geometry.

Figure 5-2. The heater (a) digital design, and (b) 3D printed (with Proto-pasta conductive PLA material and LulzBot TAZ 5 material extrusion printer).

Resistive heating is the process by which passage of current across a conductor generates heat. The amount of resistive heating may be calculated via the following equation [77]:

$$P = I^2R = V^2/R$$

This heating elevates the temperature of the resistive materials with time. To experimentally validate the performance of the printed resistive heater, an IR camera was used to capture images of the heater when 9 V was applied across the heater; images were taken right after the voltage application and after two minutes of voltage application, as shown in Figure 5-3 A and B. The images show that temperature of the heater increased with time as was expected.

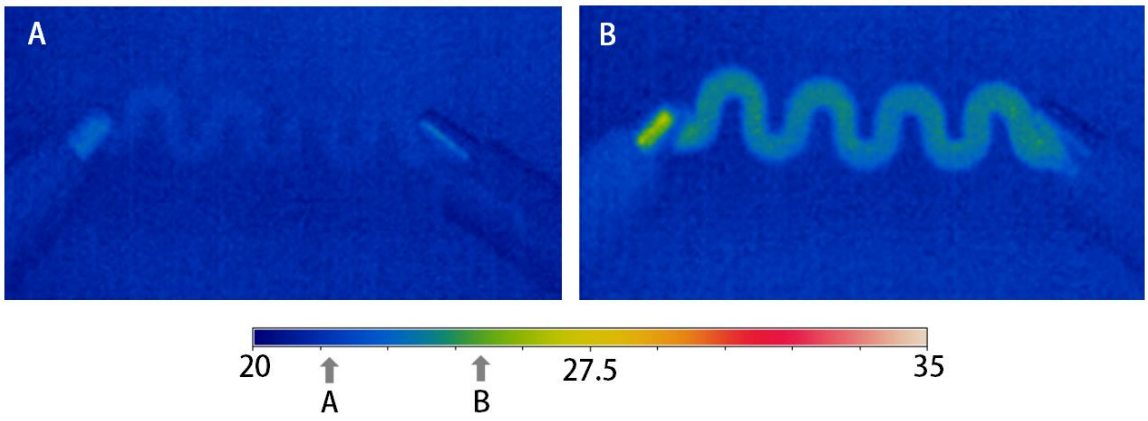

Figure 5-3. IR camera images of the heating element on applying 9 volts. 'A' shows almost no temperature change right after applying the voltage. 'B' shows the IR image of the heater after applying voltage for two minutes.

5.3 Designing the Multifunctional Component

After validating the usage of conductive PLA as a resistive heating component, the earlier DfAM findings were used to establish a geometry and embedding process for a holder capable of integrating both the resistive heater and the sun sensor. The sun sensor requires a pin hole to focus sunlight on its receptor, which means that it must be embedded just below the outside surface of the CubeSat. In order to leverage the opportunity of volume-efficient multifunctional design given by AM, a cross brace of the 3-U CubeSat (see Figure 5-4) was selected to integrate the heater and the sun sensor. Cross braces provide structural support and integrity to the structure of the CubeSat,

making them indispensable. Embedding the components would make it multi-functional, by adding the function of the sun sensor, as well as its heater.

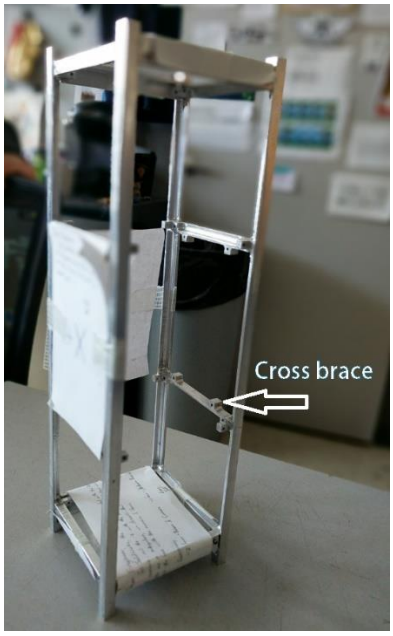

Figure 5-4. Structure of OSIRIS, the 3U CubeSat, showing the cross-brace structure that is to be designed.

The digital re-design for this cross-brace was carried out in SolidWorks™ V5. For design of the heater cavity, a negative shape of the heater was created with the appropriate clearances determined in Section 3.4: 1.25 mm in the X-Y axes for a snug fit and 0.25 mm in the Z axis for an aligned fit (see Figure 5-5 (a)). Since the heater had a flush surface and the shape converter was found to not influence the strength of the part (see Section 4.3), the heaters were directly embedded in the designed cavity. For embedding the circular disc-like sensor (see Figure 5-1), a cylindrical cavity was designed directly above the cavity for the heater; diametrically opposite risers were added to maintain the gap between the naked electrical components and the body of the holder, which prevents any damage to them (see Figure 5-5 (b)). A disc-like shape converter with a pin

hole at the center was designed in order to cover the cavity after embedding the sensor (see Figure 5-5 (c)). This was done to create a needed gap between the body of the holder and the sensor, as well as to create a flush surface for smooth and uninterrupted deposition of the resumed layer.

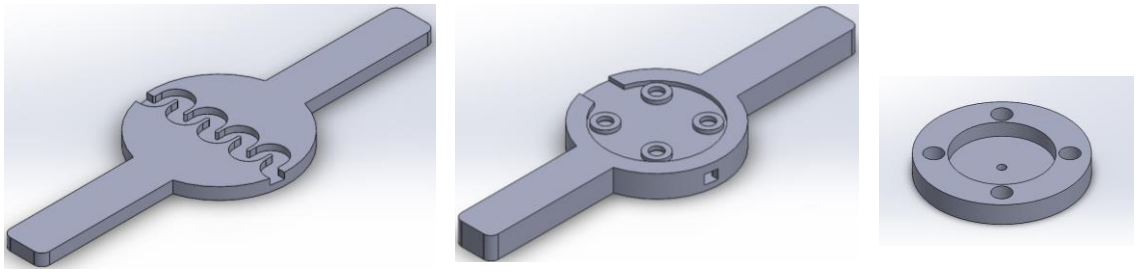

(a) (b) (c)

Figure 5-5. Isometric view of the CAD designs of the holder to embed the heater and the sun sensor. (a) shows first few layers, with the cavity designed for the heating element, (b) shows the cavity designed for the sun sensor, along with four risers, right above the cavity for the heater, (c) shows the shape converter for covering the cavity for sun sensor, with a pin hole at the center.

5.4 Manufacturing the Multi-functional Component

After the digital design was completed, MarkForged's cloud-based software (Eiger)[50] was used to prepare the print. First, the shape converter was printed since it is needed in order to complete the full component embedding in the holder. For the holder, pauses were added right after the last layer of each of the two cavities. Eiger was also prompted to add concentric carbon-fiber layers to supplement the structural integrity of the part. It should be noted that carbon fiber is partially conductive in nature, and loops of conductive material can create a magnetic flux through them. In orbit, small values of magnetic flux can cause undesired satellite attitude changes as its magnetic moment torques agains with the Earth's magnetic field. Therefore, in practice, energized loops of any conductive material should be avoided, unless required.

Another important note is that Nylon use has typically been discouraged in space applications due to its propensity to absorb water [78], which can cause undesired oxidation. Mark One printers print only Nylon as the base material. Since the emphaisis on the procedure for manufacturing the multi-functional component (rather than a specific focus on its performance in space), Nylon was used as our material, and carbon fiber loops were added for strengthening. The process of embedding is shown in Figure 5-6.

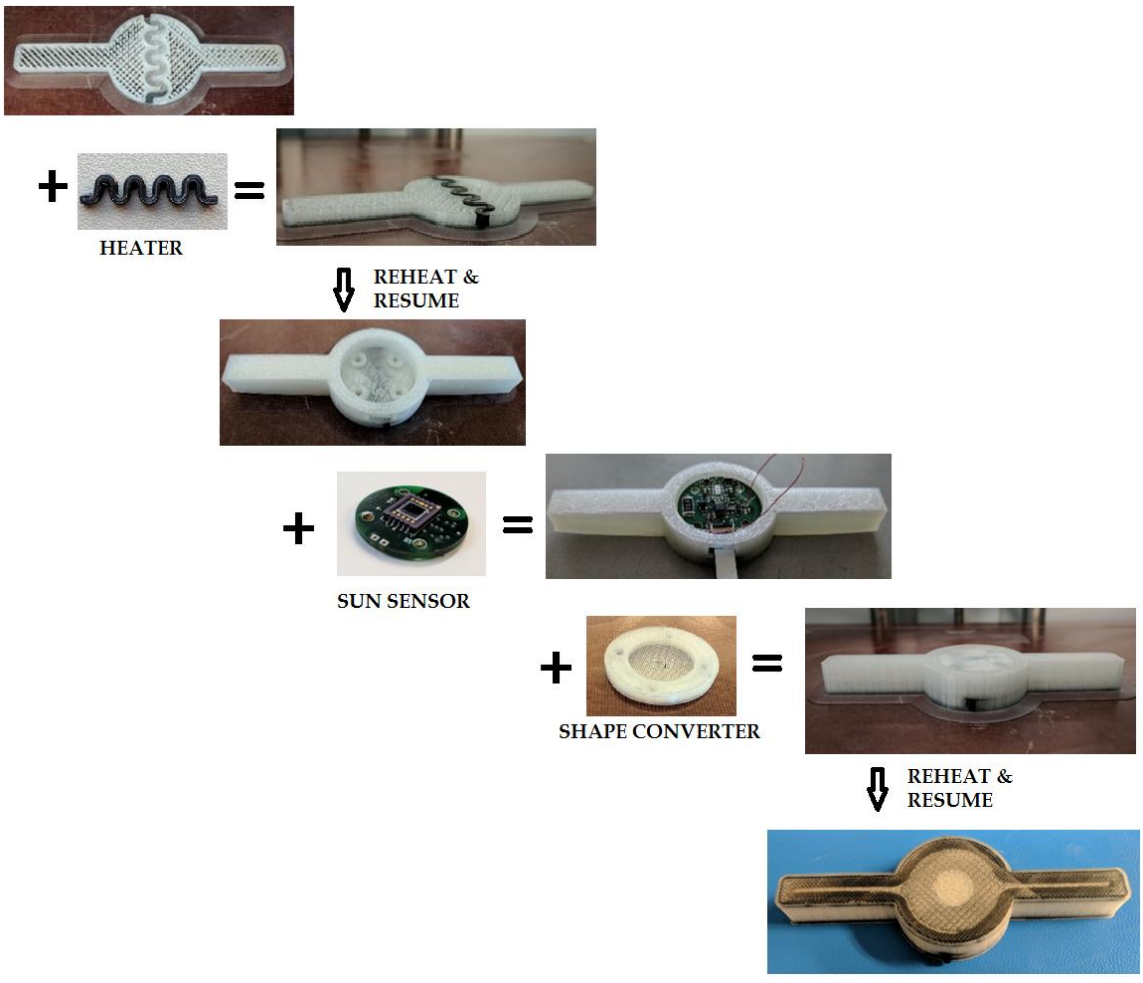

Figure 5-6. Steps of the manufacturing process of the multifunctional cross brace, where addition sign denotes the process of manually inserting the component.

Each paused step in the embedding process took approximately five minutes, which included gluing the heater into the cavity. The temperature history diagram (see Figure 3-6, in Section 3.5) from the IR camera showed that the temperature of the paused layer reduces and stabalizes within 5 minutes. Because of this, reheating of the paused layer to 110 °C was performed immediately before resuming the print, in order to mitigate the weaknesses introduced by the process interruption. As shown in Figure 5-6, the process for in-situ embedding in this case study included process interruption, component insertion, reheating and resuming of the print. Since the previous experimentation shows that process interruption introduces weaknesses in the paused layer and that it can be addressed by reheating the paused layer, this step was included in the case study process. Figure 5-7 demostrates the final structure of the OSIRIS-3U CubeSat, with the integrated multifunctional cross brace designed and manufactured in accordance with the suggested design guidelines for embedding found in this research work. This demonstrates the applicability of these guidelines, which can assist in confident application of AM in embedding.

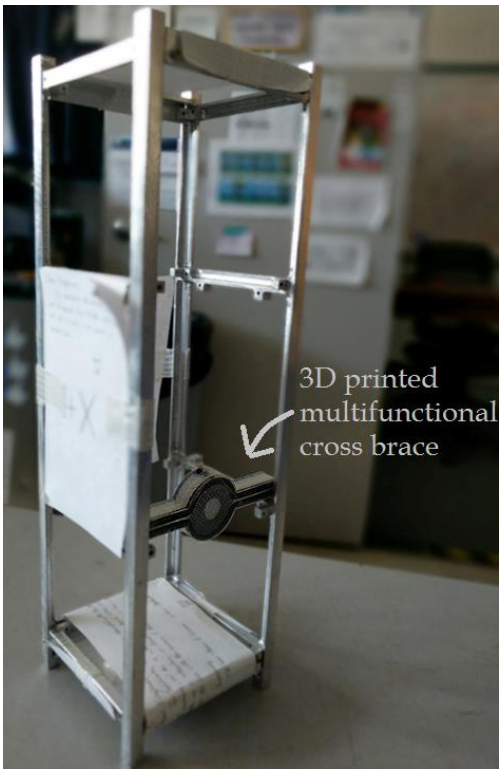

Figure 5-7. 3D printed, multifunctional cross brace structure on the three unit CubeSat.

Next chapter summarizes the findings of this research work as well as the conclusions from the case study presented.

Chapter 6

CONCLUSIONS AND FUTURE WORK

For AM embedding applications to effectively produce end-use functional products, design for AM is crucial. Design for AM involves physical design considerations for components to be embedded, as well as a deeper understanding of the manufacturing process and its effects on the strength of the part. Knowing how and where a process weakens a part is important information for decision-making during the design process. This thesis investigated the impact that the embedding parameters of process interruption and shape converter use have on the tensile strength of printed parts created via material extrusion AM. This research work provides the first known investigation of the mechanical influences of process interruption and embedding process on parts made with material extrusion, and also provides a potential solution to address identified effects.

Tensile testing specimens created to study the effects of process interruption allow the following conclusions:

- Process interruption introduces weakness at the paused layer, regardless of the time duration of pause (the maximum tensile stress value decreases significantly once the 5-minute mark is reached). The median tensile strength reduced to 48% of the non-interrupted specimens.
- The presence of an embedded component causes a significant decrease in maximum tensile stress compared to printed parts without embedded elements. The embedded material has no discernible effect on the strength of the part. The embedding causes the median stress value to be reduced to as low as 38% of the non-interrupted specimens.
- Reheating the paused layer back up to the deposition temperature before resuming the build improves the strength of parts with process interruption; the median tensile strength of reheated specimens with only process interruption improved by 47%, while reheated

embedding specimens improved by 90% when compared with their non-reheated counterparts.

These findings provide a wide scope for future research into other in-situ embedding factors, such as the effects of shape converters with different cross-sectional areas. A larger set of data for investigating the impact of process interruption length can help in better understanding the statistical abnormality observed between specimens with a 60-minute pause times and 30-minute pause time. Also, this investigation was performed for pause time durations varying from 5 minutes to 60 minutes. An investigation of shorter process interruption time durations might provide further insight into the impact of short pauses on the strength of a part. Future work should also aim to expand on the impact of material transition on strength when a print is resumed. A range of materials will be investigated for layer adhesion while embedding to provide a database of information about their influences on strength. A range of other AM process types should also be compared to see how the findings in this research can be more generally applied to different AM process. This can aid in making better decisions for material and process selection while designing for multi-functional embedding with AM.

Bibliography

[1] J. Perrin, *Concevoir l'innovation industrielle: méthodologie de conception de l'innovation*. Paris, France: CNRS Editions, 2001.

[2] S. M. Sapuan and M. R. Mansor, "Concurrent engineering approach in the development of composite products: A review," *J. Mater.*, vol. 58, pp. 161–167, 2014.

[3] S.-Y. Wu, C. Yang, W. Hsu, and L. Lin, "3D-printed microelectronics for integrated circuitry and passive wireless sensors," *Microsystems Nanoeng.*, vol. 1, no. April, pp. 1–9, 2015.

[4] T.-C. Kuo, S. H. Huang, and H.-C. Zhang, "Design for manufacture and design for 'X': concepts, applications, and perspectives," *Comput. Ind. Eng.*, vol. 41, no. 3, pp. 241–260, 2001.

[5] D. W. Rosen, "Design for additive manufacturing: A method to explore unexplored regions of the design space," in *Eighteenth Annual Solid Freeform Fabrication Symposium*, 2007, pp. 402–415.

[6] S. H. Poggenpohl and K. Sato, *Design Integrations: Research and Collaboration*. Chicago: Intellect, the University of Chicago Press, 2009.

[7] C. M. Reigeluth and T. W. Frick, "Formative research: A methodology for creating and improving design theories," *C. Reigeluth (Ed.), Instr. Theor. Model.*, no. 1990, pp. 1–28, 1999.

[8] F. Laverne, F. Segonds, N. Anwer, and M. Le Coq, "Assembly Based Methods to Support Product Innovation in Design for Additive Manufacturing: An Exploratory Case Study," *J. Mech. Des.*, vol. 137, no. 12, pp. 121701–121701, 2015.

[9] K. Paul, "Anisotropic material properties of fused deposition modeling ABS," 2002.

[10] M. Nikzad, S. H. Masood, and I. Sbarski, “Thermo-mechanical properties of a highly filled polymeric composites for Fused Deposition Modeling,” *Mater. Des.*, vol. 32, no. 6, pp. 3448–3456, 2011.

[11] A. Kumar, R. K. Ohdar, and S. S. Mahapatra, “Parametric appraisal of mechanical property of fused deposition modelling processed parts,” *Mater. Des.*, vol. 31, no. 1, pp. 287–295, 2010.

[12] K. Prashantha and F. Roger, “Multifunctional properties of 3D printed poly(lactic acid)/graphene nanocomposites by fused deposition modeling,” *J. Macromol. Sci. Part A*, vol. 54, no. 1, pp. 24–29, 2017.

[13] A. Bellini, S. Güçeri, and M. Bertoldi, “Liquefier Dynamics in Fused Deposition,” *J. Manuf. Sci. Eng.*, vol. 126, no. 2, pp. 237–246, 2004.

[14] J. Kerns, “3D Printing Tips and Tech: Get to Know Those Acronyms,” *Machine Design*, 2015. .

[15] V. Kumar, S. Rajagopalan, M. R. Cutkosky, and D. Dutta, “Representation and Processing of Heterogeneous Objects for Solid Freeform Fabrication,” *Geom. Model. Work.*, pp. 1–21, 1998.

[16] N. A. Meisel, A. M. Elliott, and C. B. Williams, “A procedure for creating actuated joints via embedding shape memory alloys in PolyJet 3D printing,” *J. Intell. Mater. Syst. Struct.*, vol. 26, no. 12, pp. 1498–1512, 2015.

[17] S. Geller and M. Gude, “Process-Integrated Manufacturing and Embedding of Novel Piezoelectric Sensor Modules into Glass Fibre-Reinforced Polyurethane Composite Structures,” *Mater. Sci. Forum*, vol. 825–826, pp. 563–570, Jul. 2015.

[18] R. R. J. Maier, W. N. MacPherson, J. S. Barton, M. Carne, M. Swan, J. N. Sharma, S. K. Futter, D. A. Knox, B. J. S. Jones, and S. McCulloch, “Embedded fiber optic sensors

within additive layer manufactured components," *IEEE Sens. J.*, vol. 13, no. 3, pp. 969–979, 2013.

[19] K. D. D. Willis, E. Brockmeyer, S. E. Hudson, and I. Poupyrev, "Printed Optics : 3D Printing of Embedded Optical Elements for Interactive Devices," *UIST '12*, pp. 589–598, 2012.

[20] B. Sterling, *Shaping Things*, vol. 39, no. 5. London, England: MEDIAWORK, The MIT Press, 2005.

[21] E. MacDonald, R. Salas, D. Espalin, M. Perez, E. Aguilera, D. Muse, and R. B. Wicker, "3D printing for the rapid prototyping of structural electronics," *IEEE Access*, vol. 2, pp. 234–242, 2014.

[22] E. Aguilera, J. Ramos, D. Espalin, F. Cedillos, D. Muse, R. Wicker, and E. MacDonald, "3D Printing of Electro Mechanical Systems," in *Proceedings of the 24th Solid Freeform Fabrication Symposium (SFF)*, 2013, pp. 950–961.

[23] K. B. Perez and C. B. Williams, "Combining Additive Manufacturing and Direct Write for Integrated Electronics – A Review," in *International Solid Freeform Fabrication Symposium Proceedings*, 2013, pp. 962–979.

[24] W. Gao, Y. Zhang, D. C. Nazzetta, K. Ramani, R. J. Cipra, and W. Lafayette, "RevoMaker : Enabling Multi-directional and Functionally-embedded 3D Printing using a Rotational Cuboidal Platform," in *Proceedings of the 28th Annual ACM Symposium on User Interface Software & Technology - UIST '15*, 2015, pp. 437–446.

[25] G. Kortuem, F. Kawsar, D. Fitton, and V. Sundramoorthy, "Smart objects as building blocks for the Internet of things," *Internet Comput. IEEE*, vol. 14, no. 1, pp. 44–51, 2010.

[26] a. C. Huebler, F. Doetz, H. Kempa, H. E. Katz, M. Bartzsch, N. Brandt, I. Hennig, U. Fuegmann, S. Vaidyanathan, J. Granstrom, S. Liu, a. Sydorenko, T. Zillger, G. Schmidt, K. Preissler, E. Reichmanis, P. Eckerle, F. Richter, T. Fischer, and U. Hahn, "Ring

oscillator fabricated completely by means of mass-printing technologies," *Org. Electron. physics, Mater. Appl.*, vol. 8, no. 5, pp. 480–486, 2007.

[27] P. Isanaka and F. Liou, "The Applications of Additive Manufacturing Technologies in Cyber Enabled Manufacturing Systems," *Proc. Annu. Int. Solid Free. Fabr. Symp. - An Addit. Manuf. Conf.*, pp. 341–353, 2012.

[28] D. Espalin, D. W. Muse, E. MacDonald, and R. B. Wicker, "3D Printing multifunctionality: Structures with electronics," *Int. J. Adv. Manuf. Technol.*, vol. 72, no. 5–8, pp. 963–978, 2014.

[29] J. Ihn and F. Chang, *Structural Health Monitoring*. 2008.

[30] M. Strantza, D. G. Aggelis, D. de Baere, P. Guillaume, and D. van Hemelrijck, "Evaluation of SHM system produced by additive manufacturing via acoustic emission and other NDT methods," *Sensors (Switzerland)*, vol. 15, no. 10, pp. 26709–26725, 2015.

[31] I. Campbell, D. Bourell, and I. Gibson, "Additive manufacturing: rapid prototyping comes of age," *Rapid Prototyp. J.*, vol. 18, no. 4, pp. 255–258, 2012.

[32] A. Kataria, D. W. Rosen, A. Kataria, and D. W. Rosen, "Building around inserts: methods for fabricating complex devices in stereolithography," *Rapid Prototyp. J.*, vol. 7, no. 5, pp. 253–262, 2001.

[33] R. Olivas, R. Salas, D. Muse, E. MacDonald, and T. Wicker, Ryan (W. M. Keck Center for 3D Innovation, The University of Texas at El Paso, El Paso, "Structural Electronics through Additive Manufacturing and Micro-Dispensing," *Int. Symp. Microelectron.*, vol. 2010, no. 1, pp. 940–946, 2010.

[34] C. Gutierrez, R. Salas, G. Hernandez, D. Muse, R. Olivas, E. MacDonald, M. D. Irwin, R. Wicker, M. Newton, K. Church, and B. Zufelt, "CubeSat Fabrication through Additive Manufacturing and Micro-Dispensing," *Int. Symp. Microelectron.*, vol. 2011, no. 1, pp. 001021–001027, 2011.

[35] C. J. Kief, B. K. Zufelt, J. H. Christensen, and J. K. Mee, “Trailblazer: Proof of Concept CubeSat Mission for SPA-1,” *AIAA Infotech*, no. March, pp. 1–7, 2011.

[36] “eoPortal Directory.” [Online]. Available: https://directory.eoportal.org/web/eoportal/satellite-missions/t/trailblazer.

[37] C. Tröger, A. T. Bens, G. Bermes, R. Klemmer, J. Lenz, and S. Irsen, “Ageing of acrylate-based resins for stereolithography: thermal and humidity ageing studies,” *Rapid Prototyp. J.*, vol. 14, no. 5, pp. 305–317, 2008.

[38] R. Hahnlen and M. J. Dapino, “Active Metal-matrix Composites with Embedded Smart Materials by Ultrasonic Additive Manufacturing,” in *SPIE Smart Structures and Materials+ Nondestructive Evaluation and Health Monitoring*, 2010, vol. 764550O-76, pp. 1–12.

[39] E. Rodriguez, J. Mireles, C. A. Terrazas, D. Espalin, M. A. Perez, and R. B. Wicker, “Approximation of absolute surface temperature measurements of powder bed fusion additive manufacturing technology using in situ infrared thermography,” *Addit. Manuf.*, vol. 5, pp. 31–39, 2015.

[40] J. Yang, S. Sun, M. Brandt, and W. Yan, “Experimental investigation and 3D finite element prediction of the heat affected zone during laser assisted machining of Ti6Al4V alloy,” *J. Mater. Process. Technol.*, vol. 210, no. 15, pp. 2215–2222, 2010.

[41] D. Schick, R. Hahnlen, and R. Dehoff, “Microstructural Characterization of Bonding Interfaces in Aluminum 3003 Blocks Fabricated by Ultrasonic Additive Manufacturing-Methods were examined to,” *Weld. ...*, no. May 2016, 2010.

[42] A. G. (The O. S. U. Truog, “Bond improvement of Al/Cu joints created by very high power ultrasonic additive manufacturing,” 2012.

[43] J. Cham, B. Pruitt, M. R. Cutkosky, M. Binnard, L. E. Weiss, and G. Neplotnik, “Layered manufacturing with embedded components: process planning considerations,”

Proceedings of DETC99: 1999 ASME Design Engineering Technical Conference. pp. 1–9, 1999.

[44] L. R. Sbriglia, A. M. Baker, J. M. Thompson, R. V Morgan, A. J. Wachtor, and J. D. Bernardin, "Embedding sensors in FDM plastic parts during additive manufacturing," in *Topics in Modal Analysis & Testing*, vol. 10, 2016, pp. 205–214.

[45] B. Stark, B. Stevenson, K. Stow-Parker, and Y. Chen, "Embedded sensors for the health monitoring of 3D printed unmanned aerial systems," *2014 Int. Conf. Unmanned Aircr. Syst. ICUAS 2014 - Conf. Proc.*, pp. 175–180, 2014.

[46] "MarkForged Mark One, world's first carbon fiber 3D printer," *www.3ders.org*, 2014. .

[47] MarkForged, "(2015) MarkForged, Mechanical Properties."

[48] F. Van Der Klift, Y. Koga, A. Todoroki, M. Ueda, and Y. Hirano, "3D Printing of Continuous Carbon Fibre Reinforced Thermo-Plastic (CFRTP) Tensile Test Specimens," no. January, pp. 18–27, 2016.

[49] G. Dumstorff and W. Lang, "Failure of Silicon Substrates Embedded in Epoxy Resin," *Procedia Technol.*, vol. 15, no. 0, pp. 216–220, 2014.

[50] "Markforged." .

[51] ASTM Norma, "Standard Test Method for Tensile Properties of Plastics," *Annu. B. ASTM Stand.*, pp. 1–15, 2004.

[52] N. I. Jaksic, "What to do when 3D printers go wrong: Laboratory experiences," *2015 122nd ASEE Annu. Conf. Expo.*, vol. 122nd ASEE, no. 2008, 2015.

[53] C. C. Seepersad, T. Govett, K. Kim, M. Lundin, and D. Pinero, "A Designer's Guide for Dimensioning and Tolerancing SLS parts," *23rd Annu. Int. Solid Free. Fabr. Symp.*, pp. 921–931, 2012.

[54] A. K. Ravi, A. Deshpande, and K. H. Hsu, “An in-process laser localized pre-deposition heating approach to inter-layer bond strengthening in extrusion based polymer additive manufacturing,” *J. Manuf. Process.*, vol. 24, pp. 179–185, 2016.

[55] “Testing for Normality using SPSS Statitics.” [Online]. Available: https://statistics.laerd.com/spss-tutorials/testing-for-normality-using-spss-statistics.php.

[56] J. H. Watt and S. van den Berg, “Selecting Statistical Tests,” in *Reserach Methods for Communication Science*, 2002, pp. 302–329.

[57] J. P. Biddix, “Research Rundowns.” [Online]. Available: https://researchrundowns.com/quantitative-methods/effect-size/.

[58] J. Bartolai, T. W. Simpson, and R. Xie, “PREDICTING STRENGTH OF THERMOPLASTIC POLYMER PARTS PRODUCED USING ADDITIVE MANUFACTURING,” 2016.

[59] “Plug and Play satellites,” *IEEE spectrum*, no. august, 2012.

[60] A. J. Lopes, E. MacDonald, and R. B. Wicker, “Integrating stereolithography and direct print technologies for 3D structural electronics fabrication,” *Rapid Prototyp. J.*, vol. 18, no. 2, pp. 129–143, 2012.

[61] R. Virk, “Modular Sun sensor system for orbital altitude determination,” The Pennsylvania State University, Schreyer Honors College, 2012.

[62] HAMATSU, “Two dimensional PSDs S5590-01 datasheet.pdf.” .

[63] B. Niese, P. Amend, S. Roth, and M. Schmidt, “Laser-based generation of conductive circuits on additive manufactured thermoplastic substrates,” *Phys. Procedia*, vol. 83, pp. 954–963, 2016.

[64] J. P. Swensen, L. U. Odhner, B. Araki, and A. M. Dollar, “Injected 3D electrical traces in additive manufactured parts with low melting temperature metals,” *Proc. - IEEE Int. Conf. Robot. Autom.*, vol. 2015-June, no. June, pp. 988–995, 2015.

[65] A. K. Sood, R. K. Ohdar, and S. S. Mahapatra, “Parametric appraisal of mechanical property of fused deposition modelling processed parts,” *Mater. Des.*, vol. 31, no. 1, pp. 287–295, 2010.

[66] J. T. Belter and A. M. Dollar, “Strengthening of 3D Printed Fused Deposition Manufactured Parts Using the Fill Compositing Technique,” no. Table 1, pp. 1–19, 2015.

[67] A. R. Torrado Perez, D. A. Roberson, and R. B. Wicker, “Fracture surface analysis of 3D-printed tensile specimens of novel ABS-based materials,” *J. Fail. Anal. Prev.*, vol. 14, no. 3, pp. 343–353, 2014.

[68] A. Dorigato, V. Moretti, S. Dul, S. H. Unterberger, and A. Pegoretti, “Electrically conductive nanocomposites for fused deposition modelling,” *Synth. Met.*, vol. 226, pp. 7–14, 2017.

[69] J. Zhang, B. Yang, F. Fu, F. You, X. Dong, and M. Dai, “Resistivity and Its Anisotropy Characterization of 3D-Printed Acrylonitrile Butadiene Styrene Copolymer (ABS)/Carbon Black (CB) Composites,” *Appl. Sci.*, vol. 7, no. 1, p. 20, 2017.

[70] M. Vatani, Y. Lu, E. D. Engeberg, and J.-W. Choi, “Combined 3D printing technologies and material for fabrication of tactile sensors,” *Int. J. Precis. Eng. Manuf.*, vol. 16, no. 7, pp. 1375–1383, 2015.

[71] N. Guo and M. C. Leu, “Additive manufacturing: Technology, applications and research needs,” *Front. Mech. Eng.*, vol. 8, no. 3, pp. 215–243, 2013.

[72] F. M. Uhl and C. A. Wilkie, “Polystyrene/graphite nanocomposites: Effect on thermal stability,” *Polym. Degrad. Stab.*, vol. 76, no. 1, pp. 111–122, 2002.

[73] J. S. Shelley, P. T. Mather, and K. L. DeVries, “Reinforcement and environmental degradation of nylon-6/clay nanocomposites,” *Polymer (Guildf).*, vol. 42, no. 13, pp. 5849–5858, 2001.

[74] M. Z. Rong, M. Q. Zhang, Y. X. Zheng, H. M. Zeng, and K. Friedrich, “Improvement of tensile properties of nano-SiO2/PP composites in relation to percolation mechanism,” *Polymer (Guildf).*, vol. 42, no. 7, pp. 3301–3304, 2001.

[75] T. Agag, T. Koga, and T. Takeichi, “Studies on thermal and mechanical properties of polyimide-clay nanocomposites,” *Polymer (Guildf).*, vol. 42, no. 8, pp. 3399–3408, 2001.

[76] “Proto-pasta: Composite PLA-ELectrically Conductive Graphite.” [Online]. Available: https://www.proto-pasta.com/collections/new-releases-favorites/products/conductive-pla.

[77] D. Ashby, *Electrical Engineering 101: Everything You Should Have Learned in School--But Probably Didn’t*. Elsevier/Newnes, 2012.

[78] F. C. Gross, “Problems Associated with Nylon Usage on Spacecraft,” 2002.